National School on Neutron and X-Ray Scattering

Neutron Reflectometry (NR)

August 2023

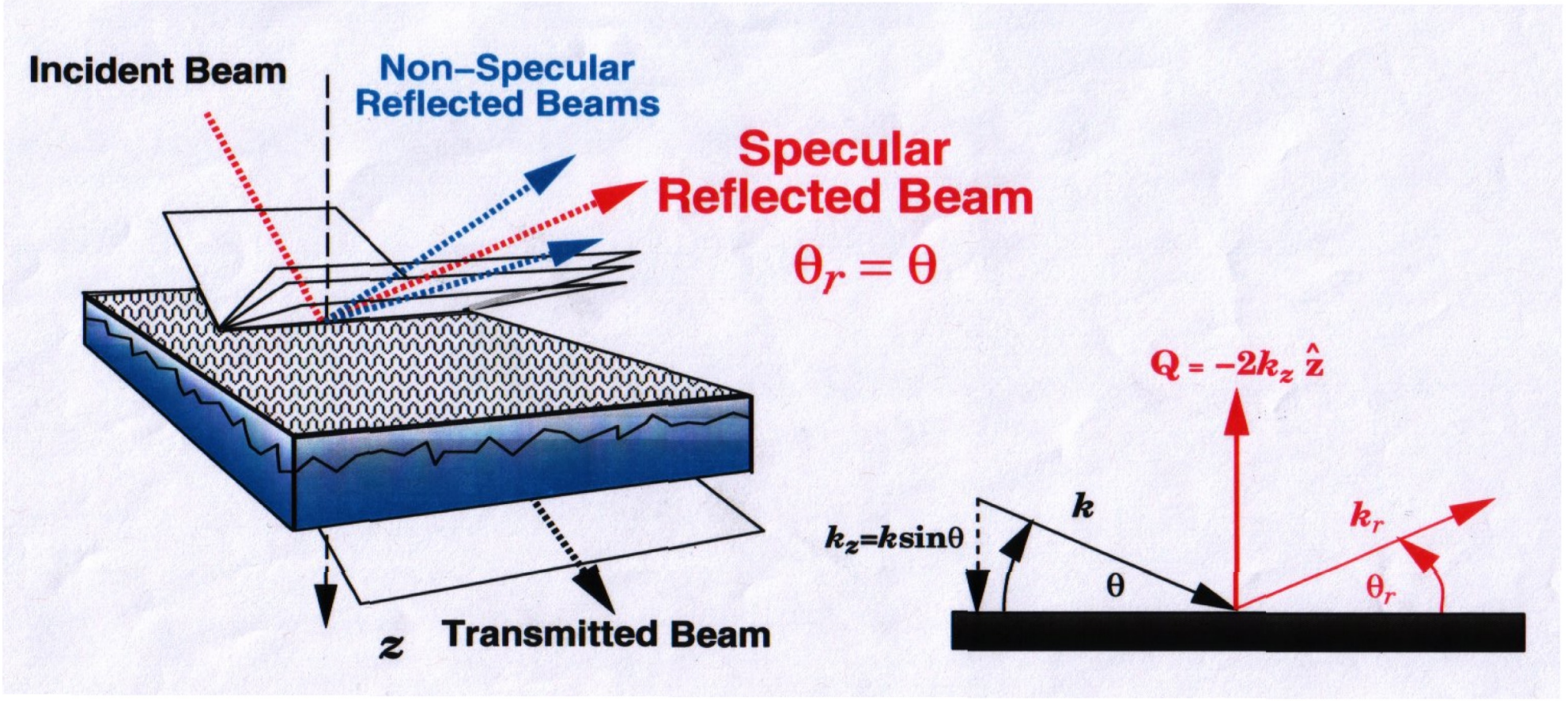

(Figure courtesy of Norm Berk)

C.F.Majkrzak, *NIST Center for Neutron Research*,
Gaithersburg, MD

NIST CENTER FOR NEUTRON RESEARCH

CHRNS CENTER FOR HIGH RESOLUTION NEUTRON SCATTERING

From real space images and geometrical optics to wave behavior and diffraction patterns:

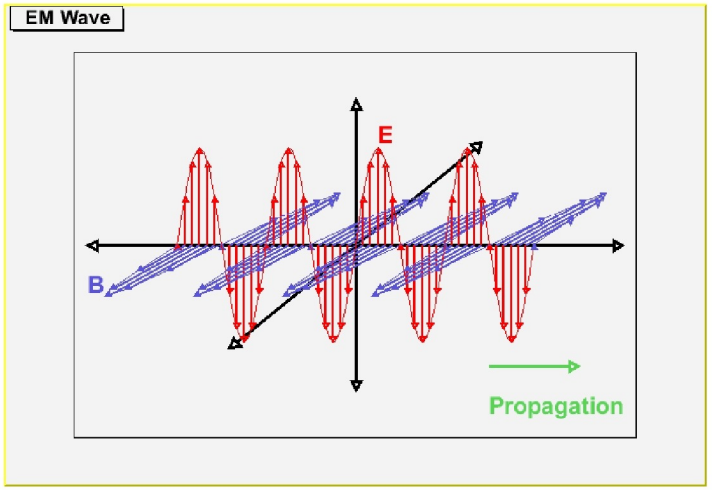

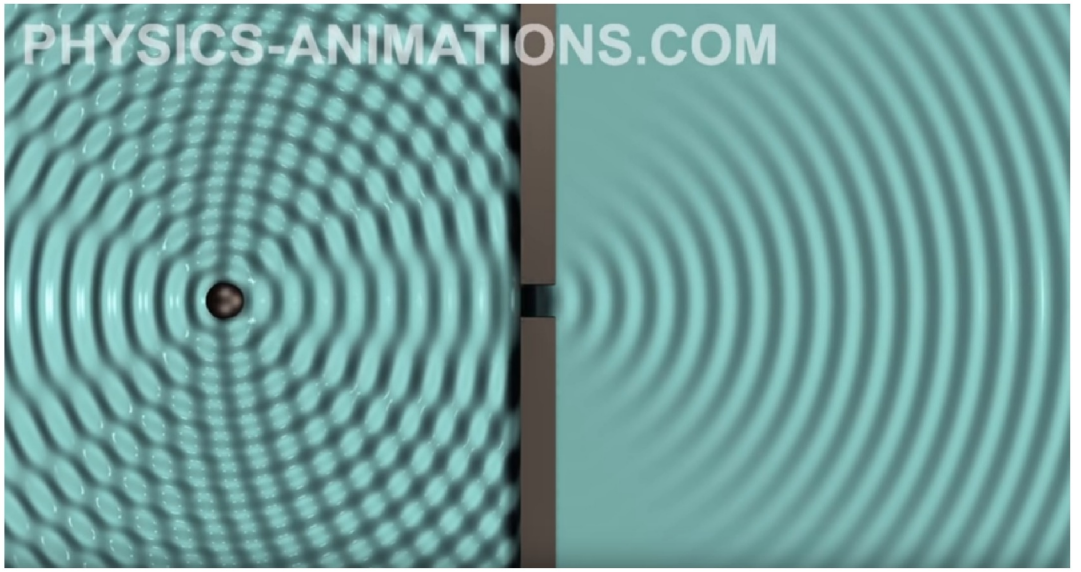

(physics.indiana.edu)

$$r(k) = [4\pi/(i2k_z S)] \int \Psi(\mathbf{k})\, \rho(\mathbf{r})\, e^{i\mathbf{k}\cdot\mathbf{r}}\, d^3r$$

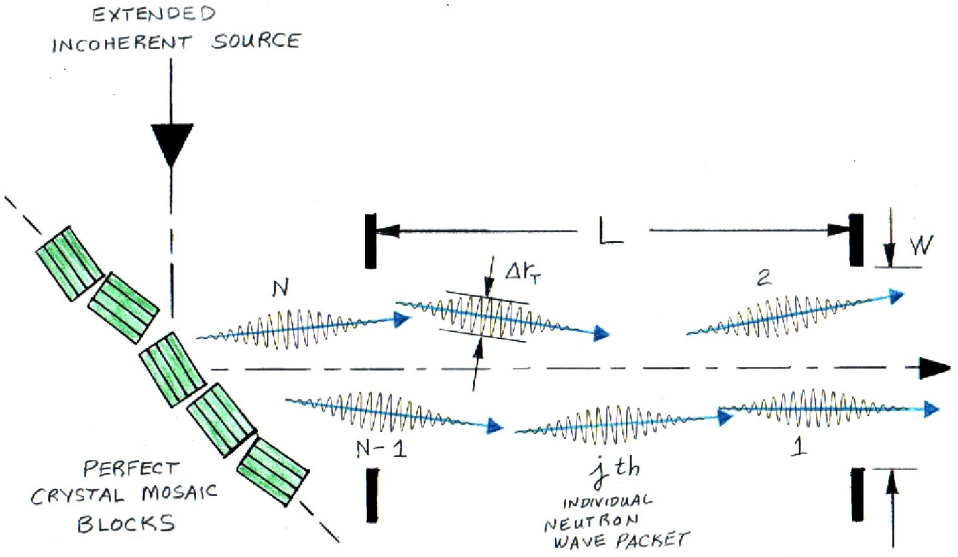

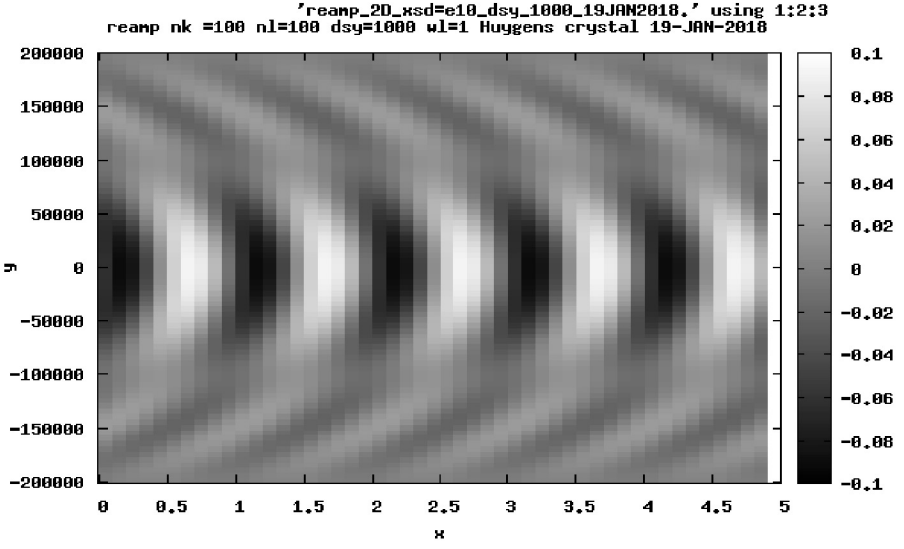

the neutron wave packet – a particle probe with a built-in ruler

Principal Uses and Advantages of Neutron Reflectometry (NR):

* For the specular condition, provides the chemical (isotopic) scattering length density (SLD) depth profile along the surface normal with a spatial resolution approaching half a nanometer.

* With polarized neutrons, provides the *vector* magnetization depth profile of a ferromagnetic material.

* Isotopic contrast, particularly applicable to hydrogen and deuterium.

* A non-destructive probe which can penetrate macroscopic distances through single crystalline substrates, making possible reflection studies of films in contact with liquids within a closed cell.

* As a consequence of the relatively weak interaction between the neutron and material, a remarkably accurate theoretical description of the reflection process and quantitative analysis of the data is possible, although the Born approximation is often not valid and an “exact” or “dynamical” formulation is required.

* NR is an established probe of the nanometer scale structure of both hard and soft condensed matter lamellar systems of interest in physics, chemistry, biology, and polymer and materials science

Part 1: Basic neutron reflectometry (NR) concepts

Part 2: Applications of specular NR to studies of the nano-scale structure of layered thin film materials

Part 3: The phase problem, direct inversion and simultaneous fitting – including an example of how a unique solution for a physical structure can be obtained

$$\text{Reflectivity} = \frac{\text{Number of reflected neutrons}}{\text{Number of incident neutrons}} = |r|^2$$

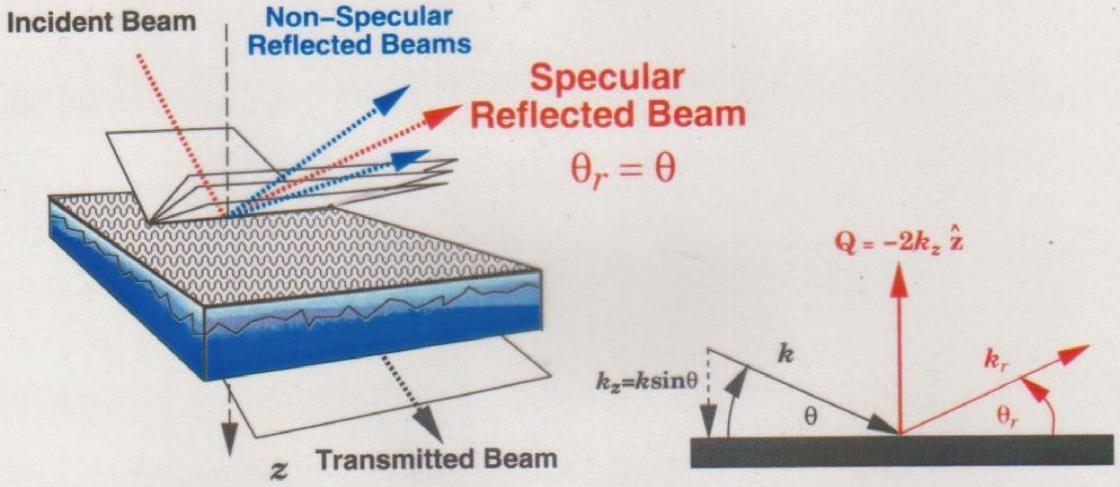

Specular reflection: $\bar{\rho}(z) = \langle \rho(x,y,z) \rangle_{xy}$

Non–Specular reflection: $\Delta\rho(x,y,z) = \rho(x,y,z) - \bar{\rho}(z)$

(AFTER N.F.BERK ET AL.)

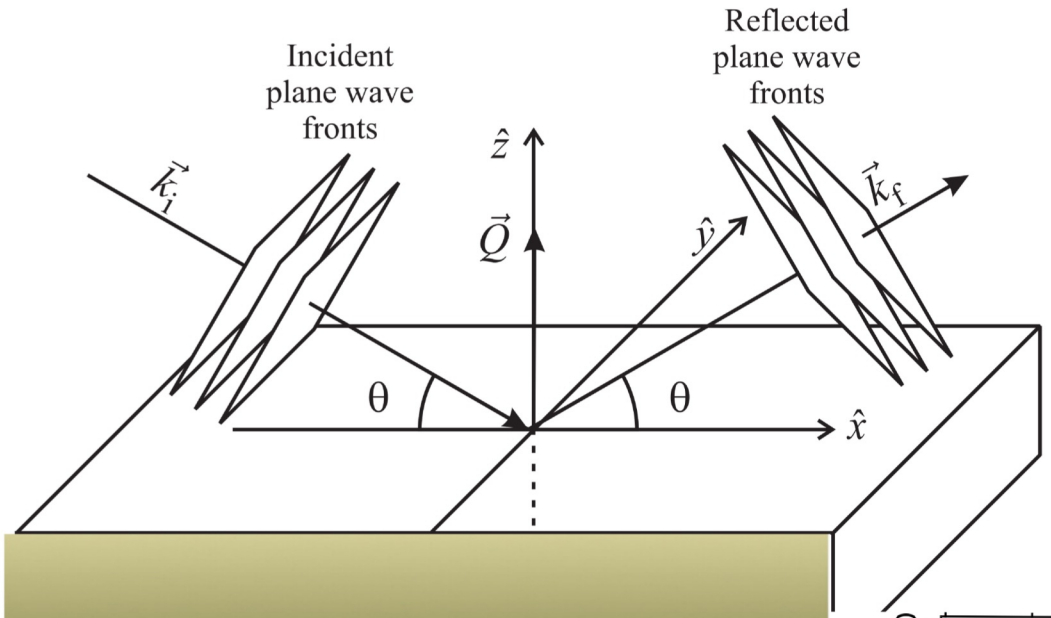

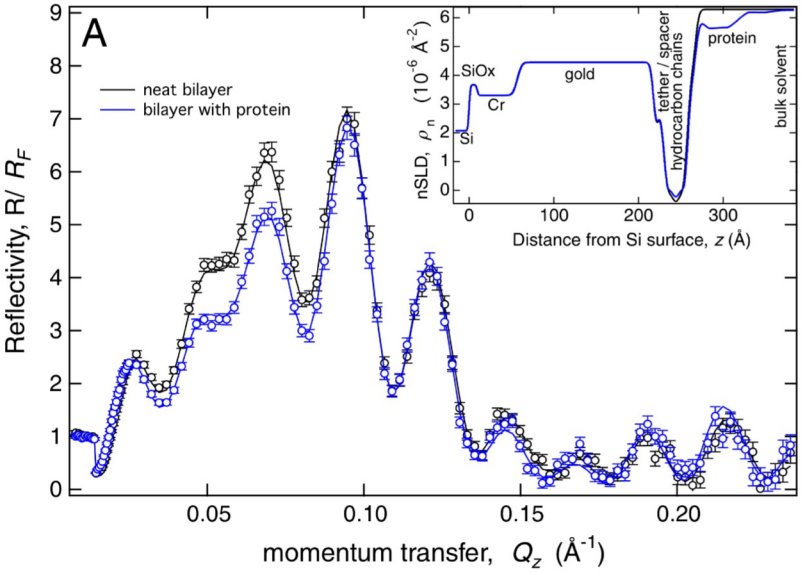

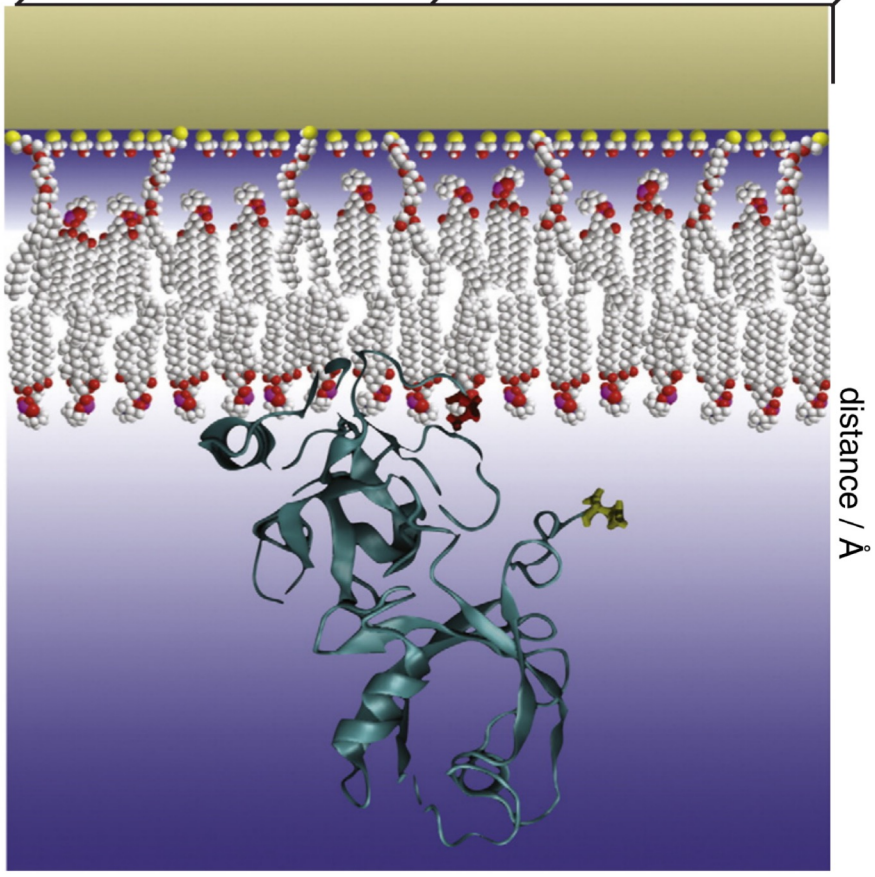

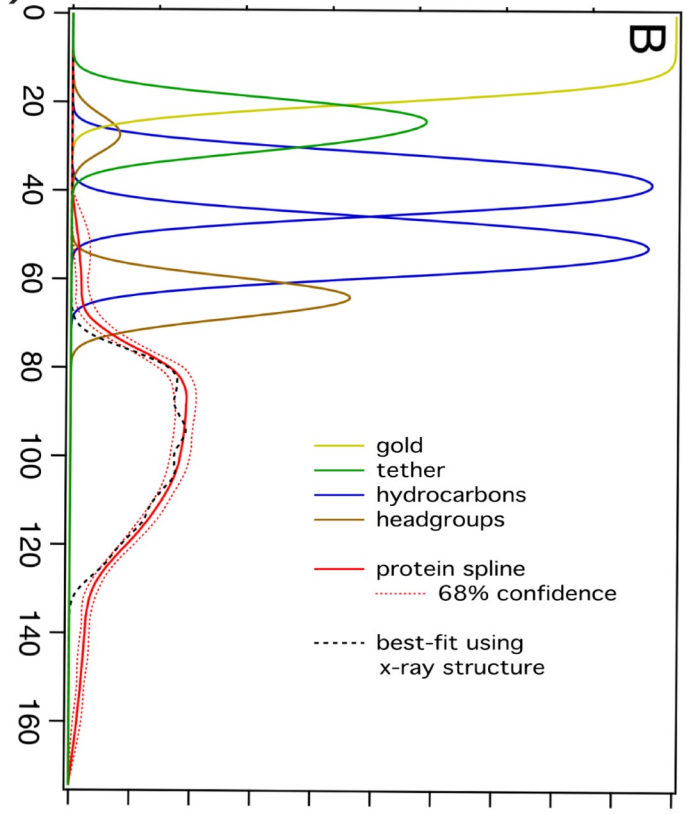

F. Heinrich, M. Lösche / Biochimica et Biophysica Acta 1838 (2014) 2341–2349

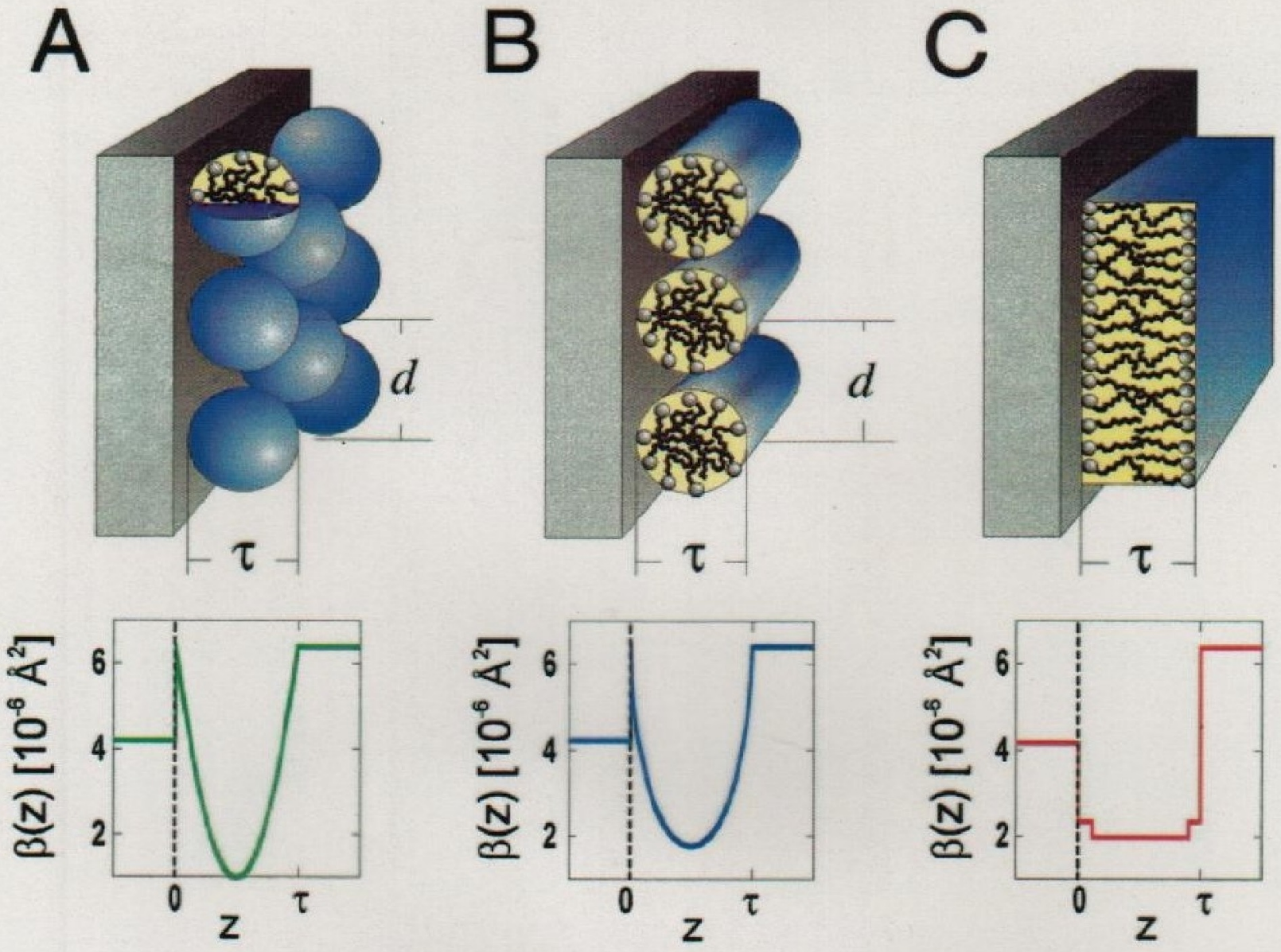

FIG. 1. (Color) Schematic diagram of adsorbed layer structures consisting of (A) spherical micelles, (B) cylindrical micelles, and (C) a bilayer, including the film thickness τ and interaggregate spacing d. Also shown are examples of neutron scattering length density profiles normal to the interface, $\beta(z)$, corresponding to each structure at the quartz/D_2O interface at a fractional surface coverage of 0.55. The head-group and alkyl tails of the surfactants have different scattering length densities, but because of the arrangement of the molecules this is only apparent in the bilayer $\beta(z)$.

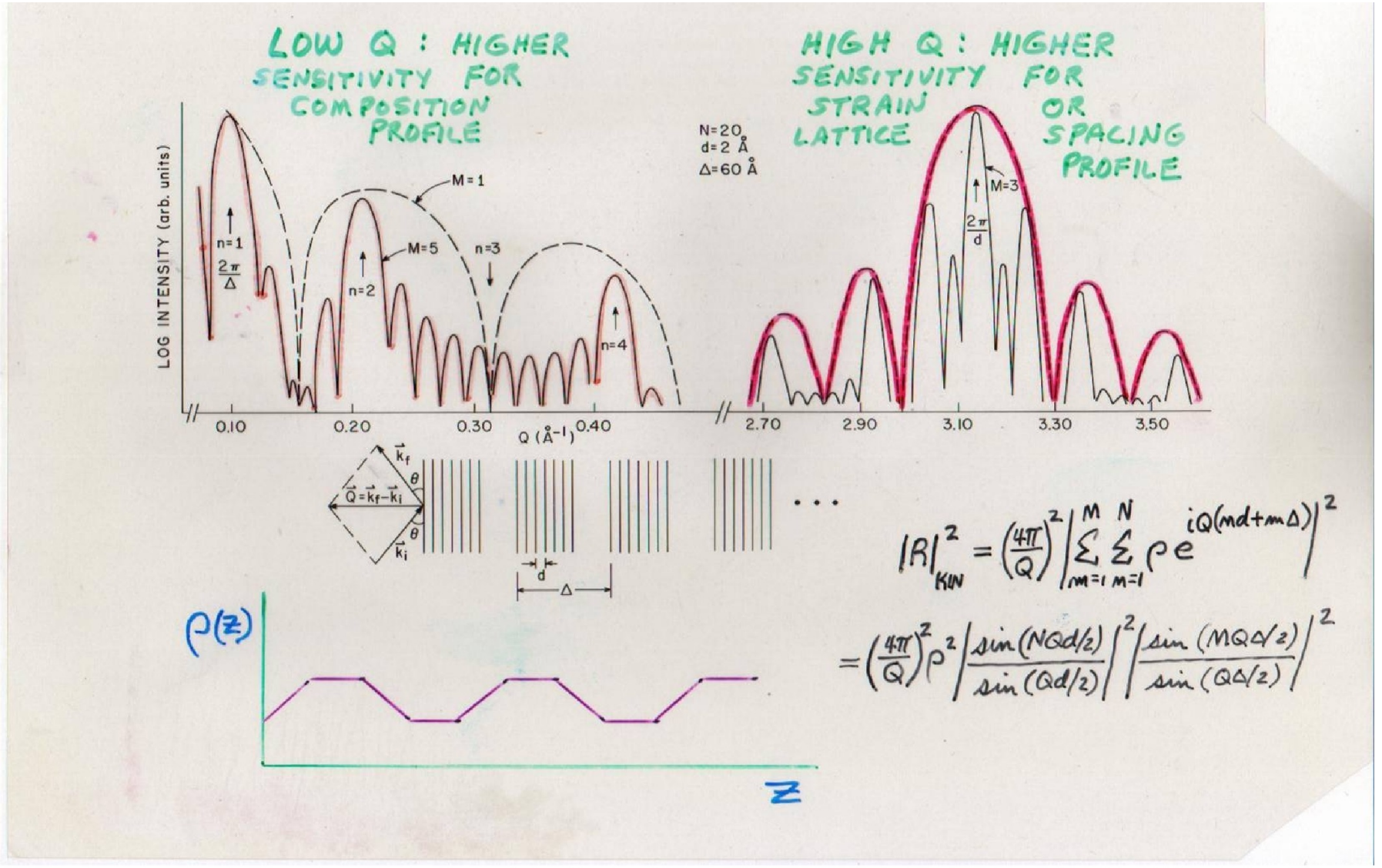

$$|R|^2_{KIN} = \left(\frac{4\pi}{Q}\right)^2 \left| \sum_{m=1}^{M} \sum_{M=1}^{N} \rho e^{iQ(md+m\Delta)} \right|^2$$

$$= \left(\frac{4\pi}{Q}\right)^2 \rho^2 \left| \frac{\sin(NQd/2)}{\sin(Qd/2)} \right|^2 \left| \frac{\sin(MQ\Delta/2)}{\sin(Q\Delta/2)} \right|^2$$

Specular reflectivity measurements are conventionally taken to mean elastic diffraction over a region of sufficiently low values of Q that sensitivity to structure at inter-atomic length scales is insignificant. Continuing a specular scan to high enough Q eventually allows the interatomic structure of, say, a superlattice to be revealed.

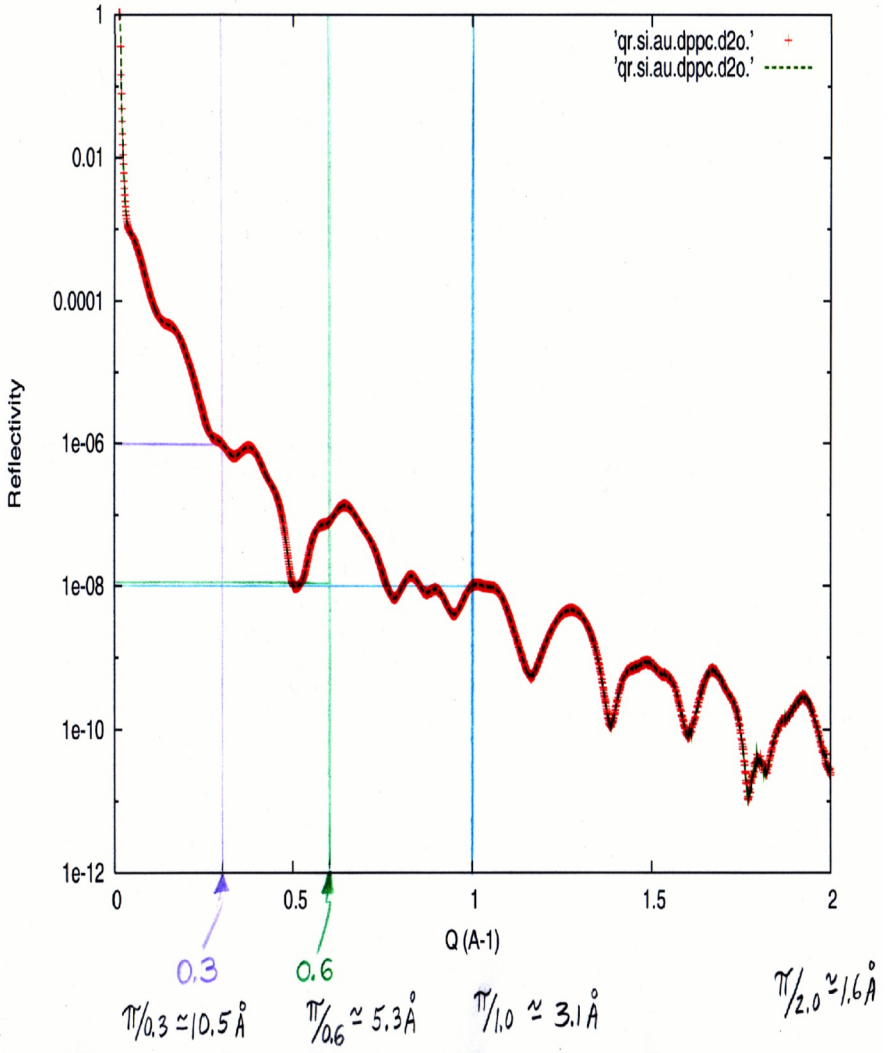

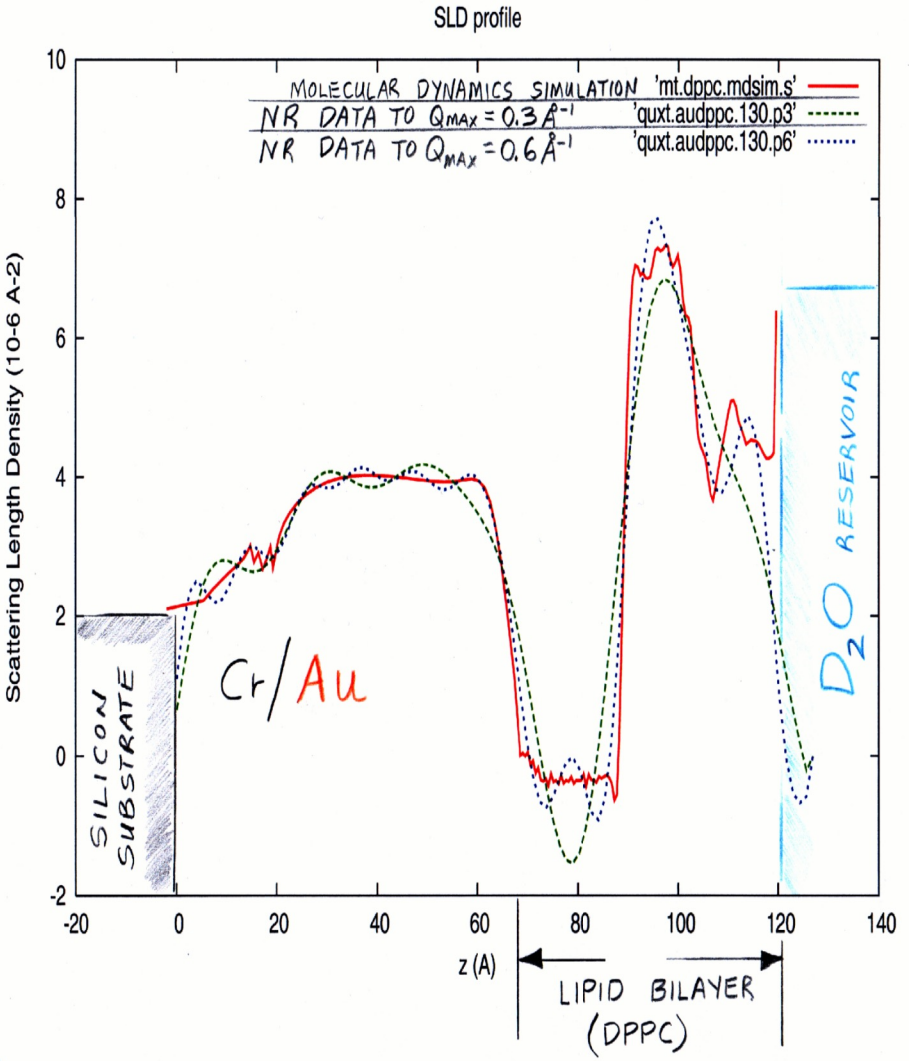

Illustration of the inverse relationship between the maximum value of Q up to which the reflectivity is measured and the spatial resolution in the corresponding SLD depth profile. Resolving smaller features in the profile in real space requires collecting reflectivity data up to larger values of Q in reciprocal space. The statistical accuracy in the measured reflectivity also affects the level of uncertainty in the associated SLD profile model to which the reflectivity data are fit.

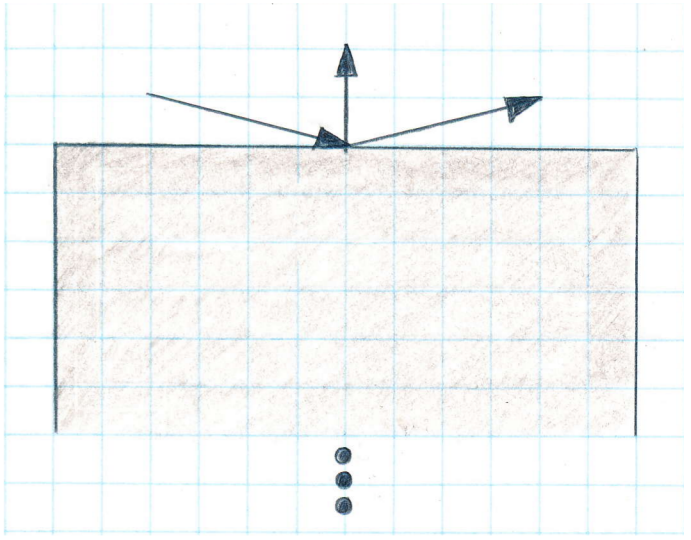

Reflection from the surface of a semi-infinite homogeneous block or “slab” of material (a possible substrate).

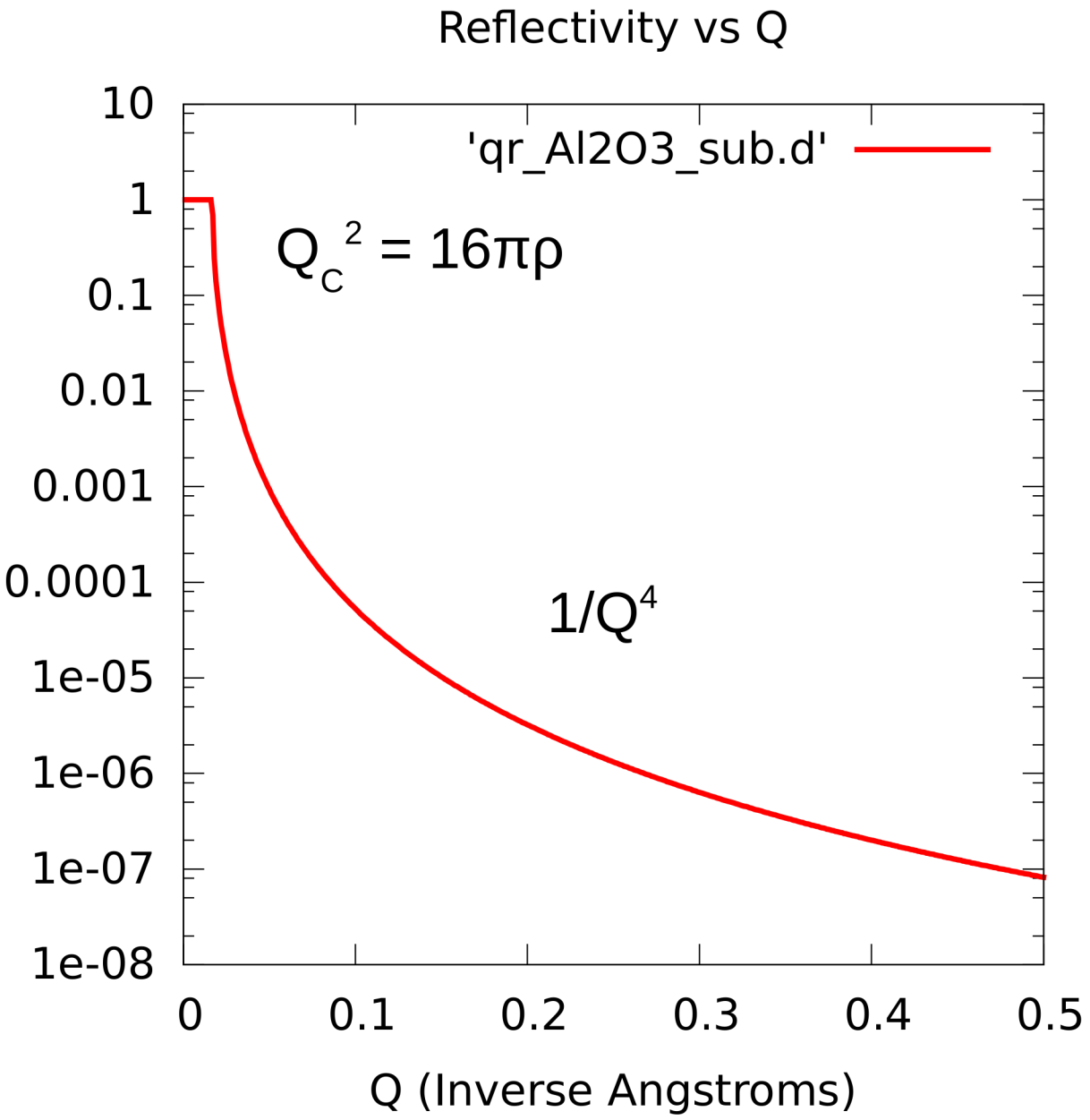

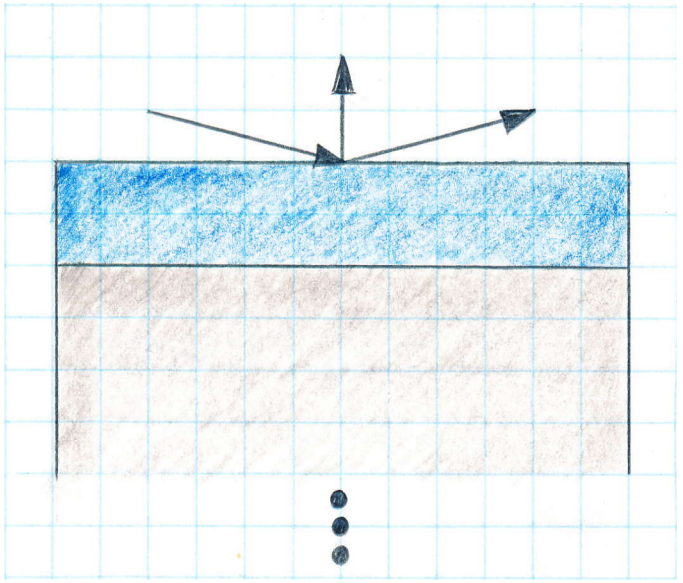

Layer of thickness D on semi-infinite substrate or “backing”.

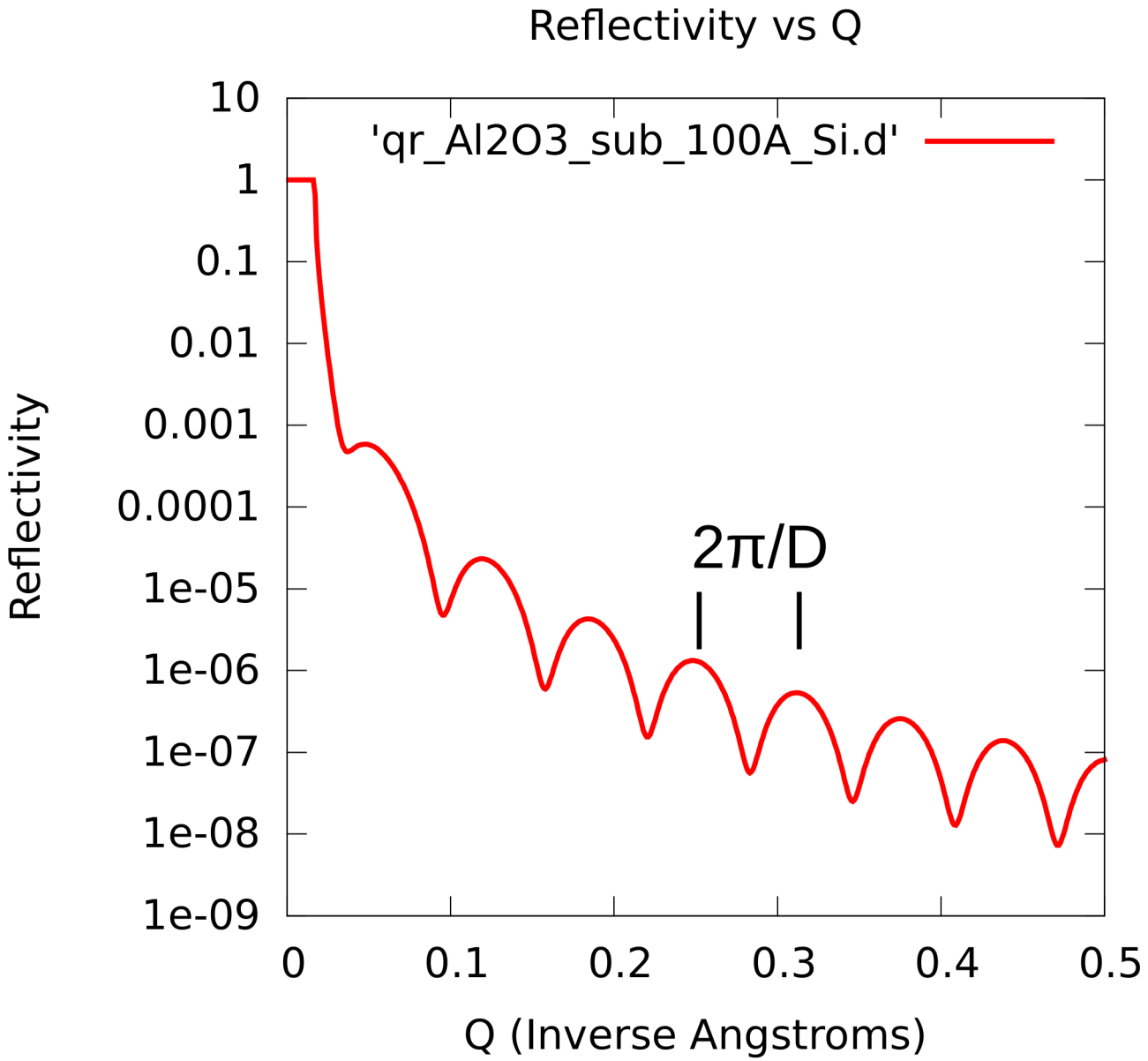

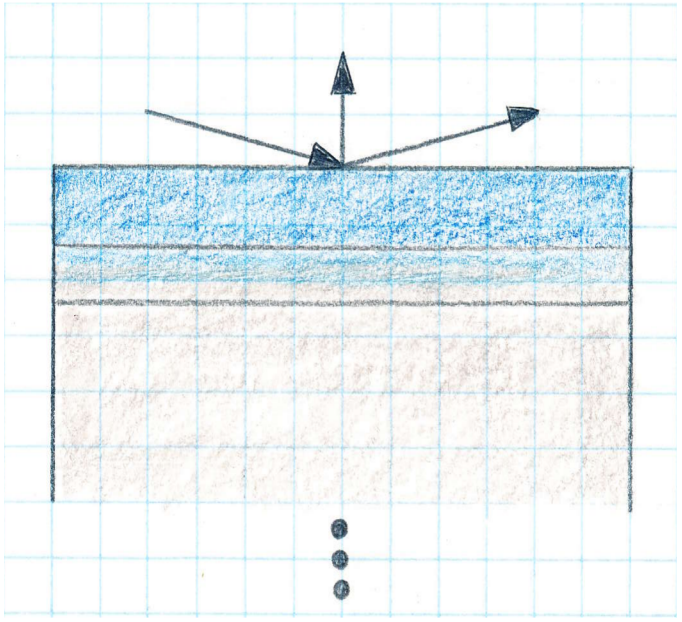

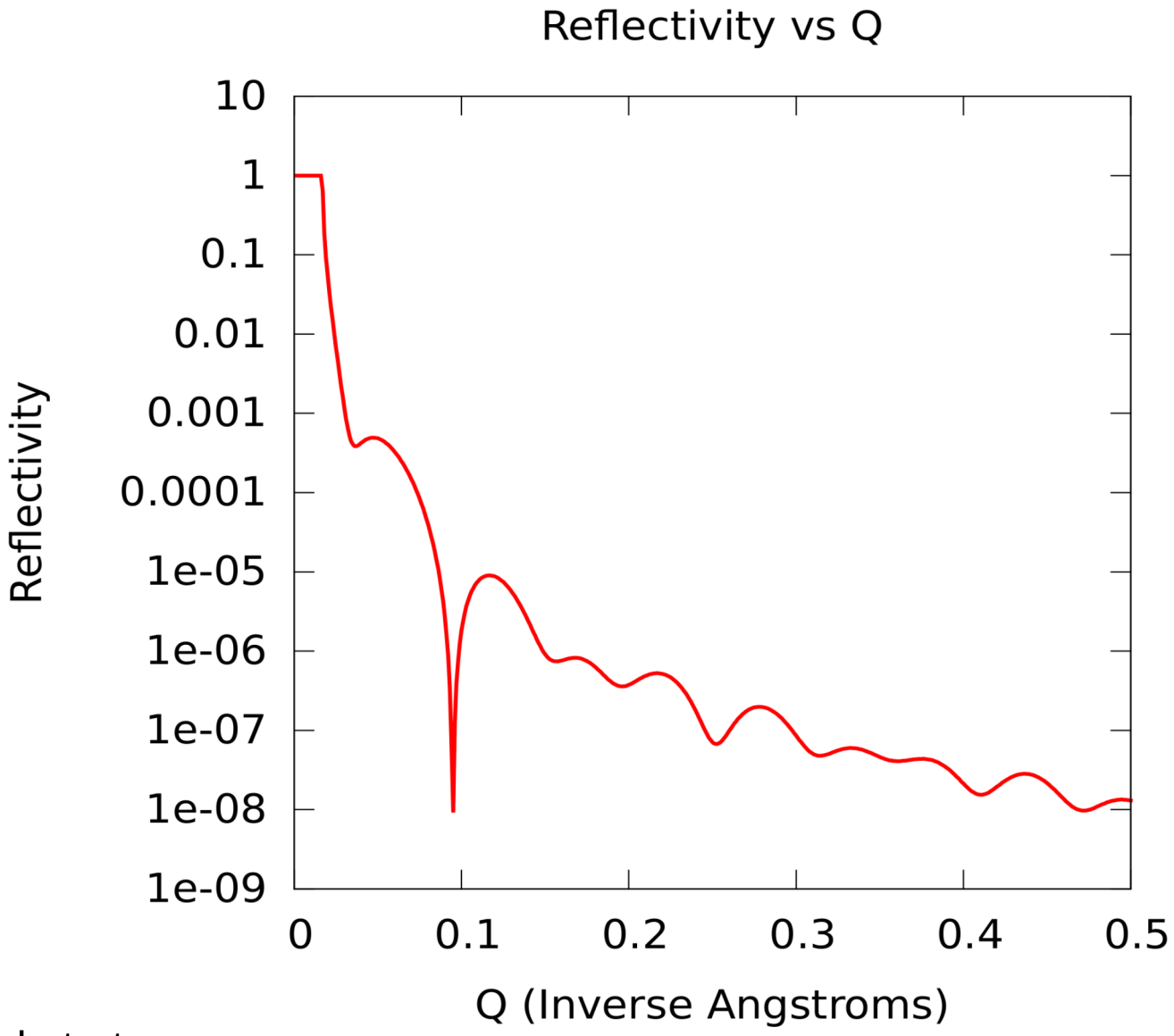

Interfacial region with gradually varying SLD between film and substrate.

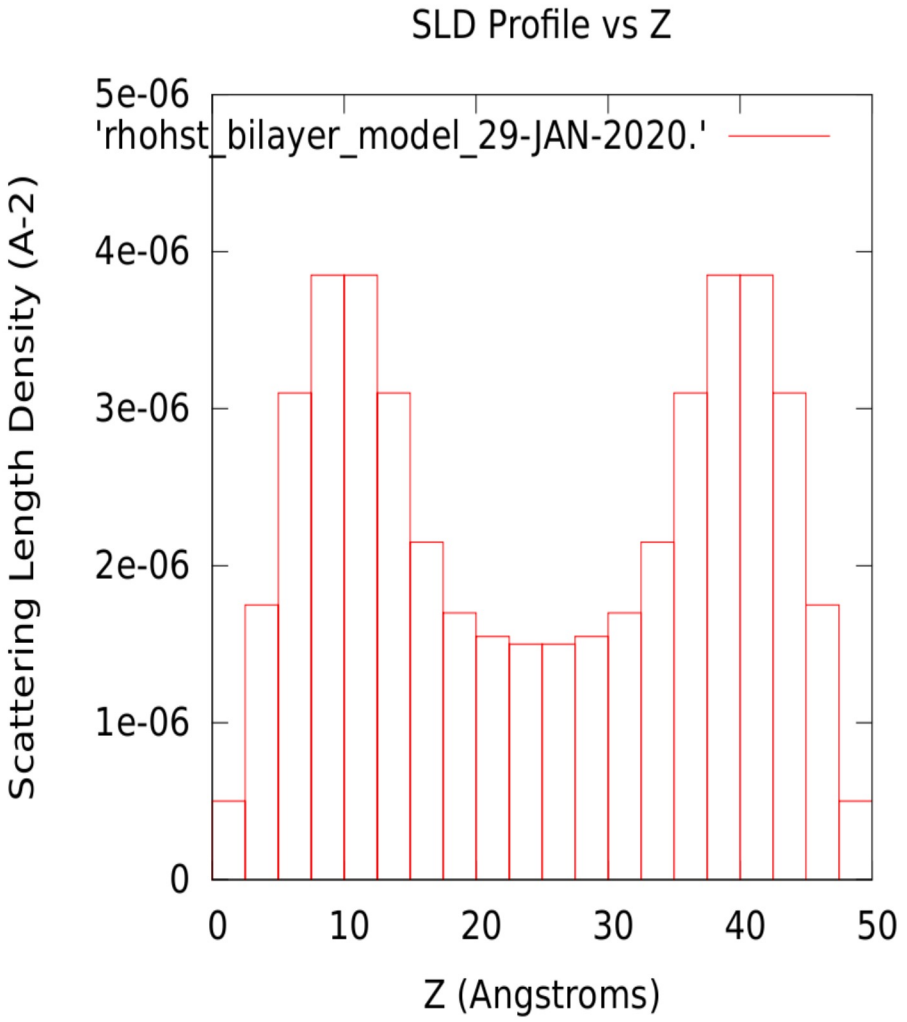
SLD Profile vs Z
'rhohst_bilayer_model_29-JAN-2020.'
Scattering Length Density (A-2)
Z (Angstroms)
5e-06
4e-06
3e-06
2e-06
1e-06
0
0
10
20
30
40
50

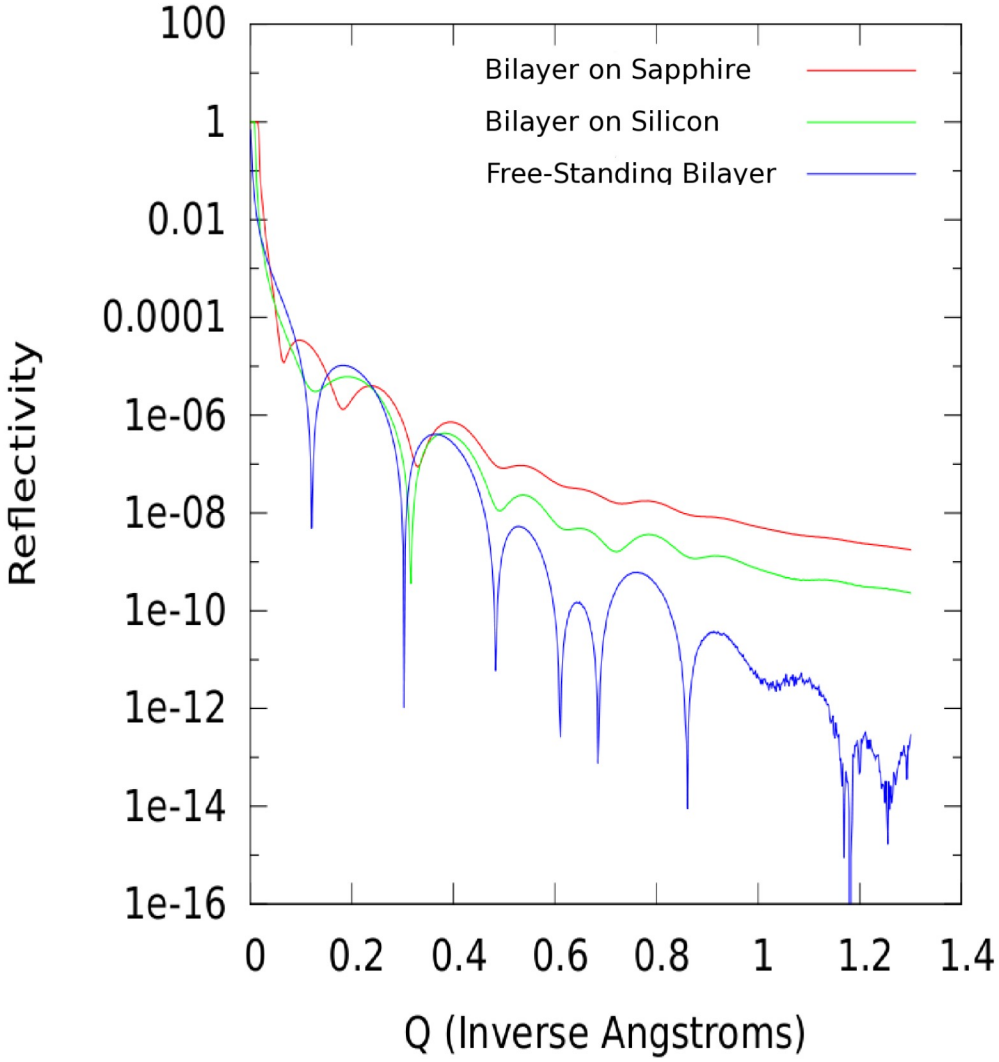
Bilayer on Sapphire
Bilayer on Silicon
Free-Standing Bilayer
Reflectivity
Q (Inverse Angstroms)
100
1
0.01
0.0001
1e-06
1e-08
1e-10
1e-12
1e-14
1e-16
0
0.2
0.4
0.6
0.8
1
1.2
1.4

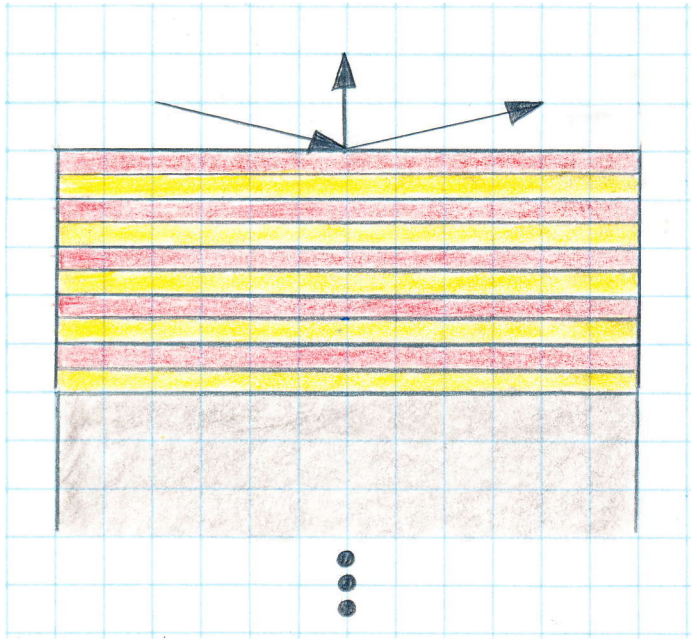

Periodic multilayer film system in which alternating layers of two different SLDs are of equal thickness.

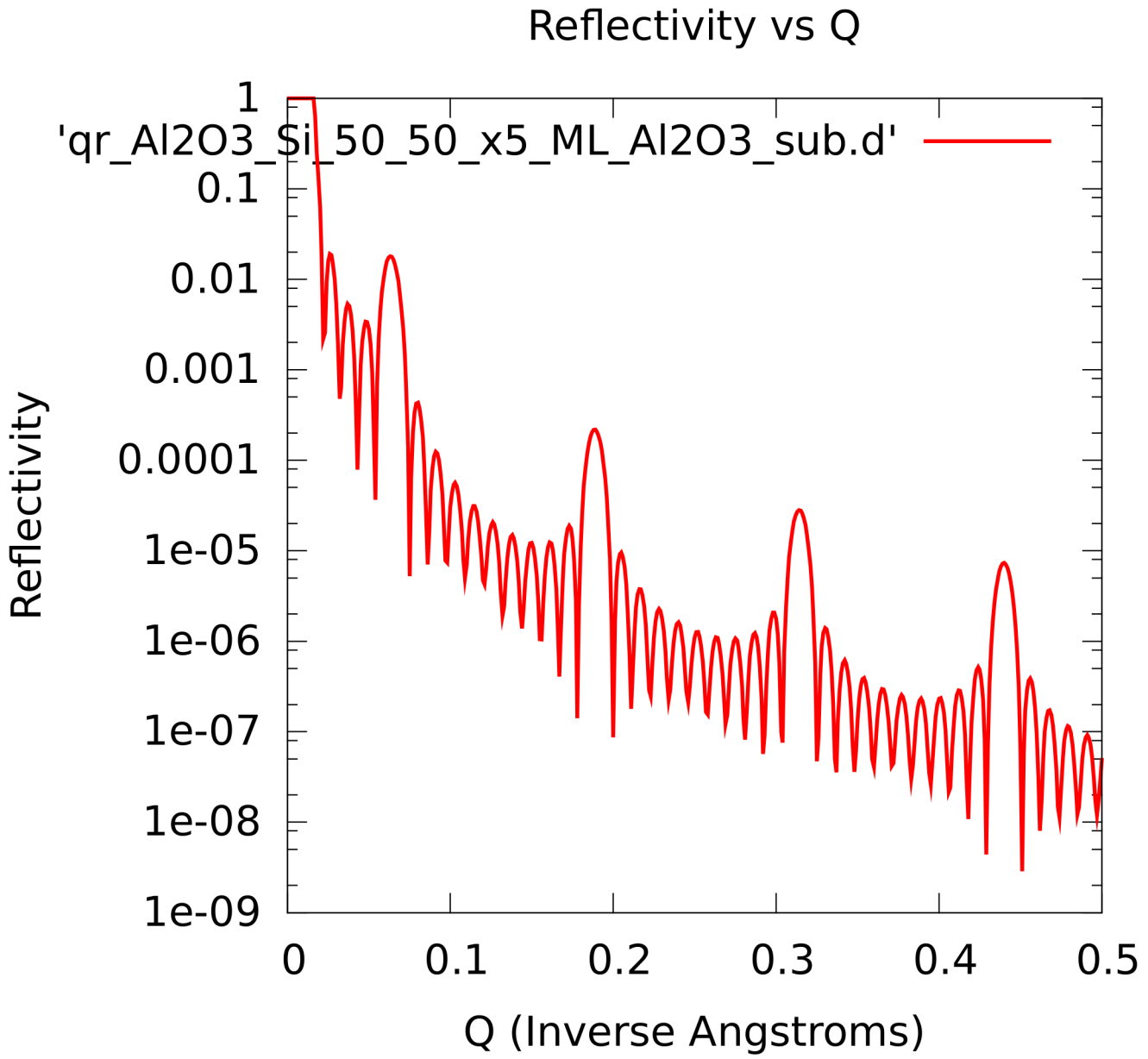

Specular Reflectivity

The reflection *amplitude* $r(Q_Z)$ is expressed as

$$r(Q_Z) = [4\pi / (iQ_Z)] \int_{-\infty}^{+\infty} \psi(z)\, \rho(z)\, \exp(-ik_{Fz}z)\, dz$$

where $\psi(z)$ represents the wave function everywhere within the scattering potential. The exponential $\exp(-ik_{Fz}z)$ represents the outgoing wavefunction. In the first Born approximation (BA), $\psi(z)$ is replaced with a wave function of the form of an undistorted incident plane wave $\exp(+ik_{Iz}z)$. Substituting $Q_Z = k_{Fz} - k_{Iz}$, we obtain

$$r_{BA}(Q_Z) \approx [4\pi / (iQ_Z)] \int_{-\infty}^{+\infty} \rho(z)\, \exp(-iQ_z z)\, dz$$

THE NEUTRON AS A PLANE WAVE PROPAGATING IN FREE SPACE

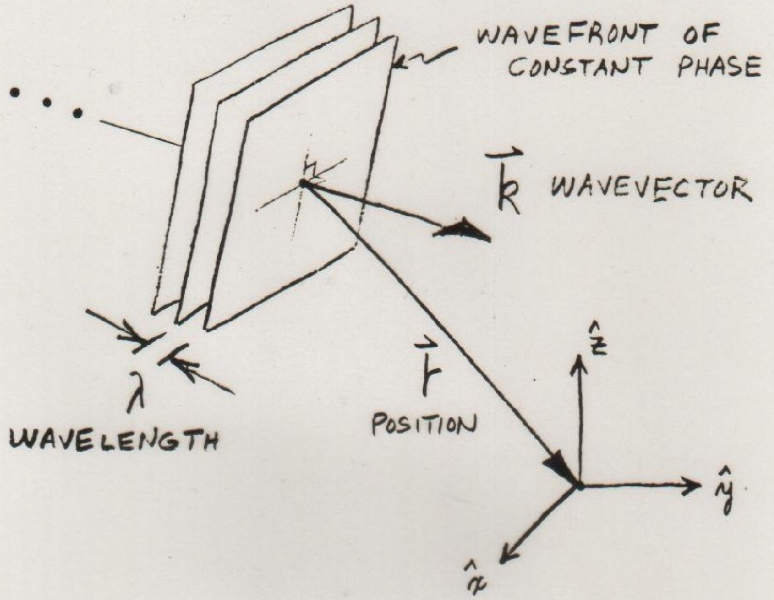

WAVEFUNCTION

$$\Psi \propto e^{i \vec{k}_0 \cdot \vec{r}}$$

$$\begin{cases} \vec{k}_0 = k_{0x}\hat{x} + k_{0y}\hat{y} + k_{0z}\hat{z} \\ \vec{r} = x\hat{x} + y\hat{y} + z\hat{z} \end{cases}$$

FOR $\vec{k}_0$ ALONG $\hat{z}$, FOR EXAMPLE,

$$\Psi \propto \cos(k_{0z} z) + i \sin(k_{0z} z)$$

$$= \left(\frac{2\pi}{\lambda} z\right)$$

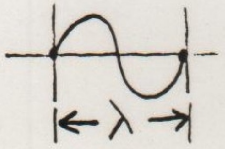

$|\Psi|^2 \propto$ PROBABILITY OF THE NEUTRON BEING THERE

FOR ELASTIC INTERACTIONS
TOTAL ENERGY OF THE
NEUTRON IS CONSTANT

TOTAL ENERGY = KINETIC ENERGY
+ POTENTIAL ENERGY

= CONSTANT

WAVE EQUATION OF MOTION
(SCHROEDINGER EQUATION)

$$\underbrace{\left[\frac{-\hbar^2}{2m}\nabla^2\right]}_{\text{K.E.}} + \underbrace{V(\vec{r})}_{\text{P.E.}}\Psi = \underbrace{E}_{\text{T.E.}}\Psi$$

$$\nabla^2 = \frac{\partial^2}{\partial x^2} + \frac{\partial^2}{\partial y^2} + \frac{\partial^2}{\partial z^2}$$

IN VACUUM

$$\text{K.E.}_0 = \frac{\hbar^2 k_0^2}{2m}$$

IN THE CONTINUUM LIMIT

$$V(\vec{r}) = \frac{2\pi\hbar^2}{m} \sum_{j=1} N_j b_j = \frac{2\pi\hbar^2}{m} \rho$$

N_j: NUMBER OF ATOMS OF TYPE j PER UNIT VOLUME

b_j: COHERENT SCATTERING LENGTH OF ATOM j —

$$b = \underbrace{\mathrm{Re}\, b}_{\text{SCATTERING}} + i \underbrace{\mathrm{Im}\, b}_{\text{ABSORPTION}}$$

ρ: SCATTERING LENGTH DENSITY (SLD)

IN VACUUM

$$E_0 = \frac{\hbar^2 k_0^2}{2m} + 0$$

IN A MATERIAL MEDIUM

$$E = \frac{\hbar^2 k^2}{2m} + \frac{2\pi\hbar^2}{m} \rho$$

CONSERVATION OF ENERGY REQUIRES $E_0 = E$

SO THAT

$$k^2 = k_0^2 - 4\pi\rho$$

& THEREFORE

$$\boxed{[\nabla^2 + k^2]\Psi = 0}$$

CAN THEN DEFINE A REFRACTIVE INDEX $n \equiv \frac{k}{k_0}$

OR

$$\boxed{n^2 = 1 - \frac{4\pi\rho}{k_0^2}}$$

Expanding $k^2 = k_0^2 - 4\pi\rho$, $k_x^2 + k_y^2 + k_z^2 + 4\pi\rho = k_{0x}^2 + k_{0y}^2 + k_{0z}^2$. Now if $\rho = \rho(z)$ only, then $\partial\rho/\partial x$ and $\partial\rho/\partial y$, which are proportional to the gradients of the potential or forces in the respective directions, are equal to zero. Thus, no force acts along these directions to change k_x and k_y . Then $k_x = k_{0x}$ and $k_y = k_{0y}$ are "constants of the motion". Substituting $\Psi(\mathbf{r}) = \exp(ik_{0x}x)\exp(ik_{0y}y)\psi(z)$ into $[\text{grad}^2 + k^2]\,\Psi = 0$ gives

$[\partial^2/\partial z^2 + k_z^2]\psi(z) = 0$ where $k_z^2 = k_{0z}^2 - 4\pi\rho(z)$.

Because there is no change in the potential in the x- or y-direction, there can be no momentum changes in these directions either. The ideal slab geometry with $\rho = \rho(z)$ only thus gives rise to the coherent "specular" reflection of a plane wave which is described by a one-dimensional wave equation:

$$[\partial^2/\partial z^2 + k_{0z}^2 - 4\pi\rho(z)]\psi(z) = 0$$

In this specular case, $\theta_I = \theta_F = \theta$, $|\mathbf{k_I}| = |\mathbf{k_F}|$, and $Q = 2k\sin\theta = 2k_z$. Also, a refractive index can n_z can be defined through $n_z^2 = 1 - 4\pi\rho(z)/k_{0z}^2$.

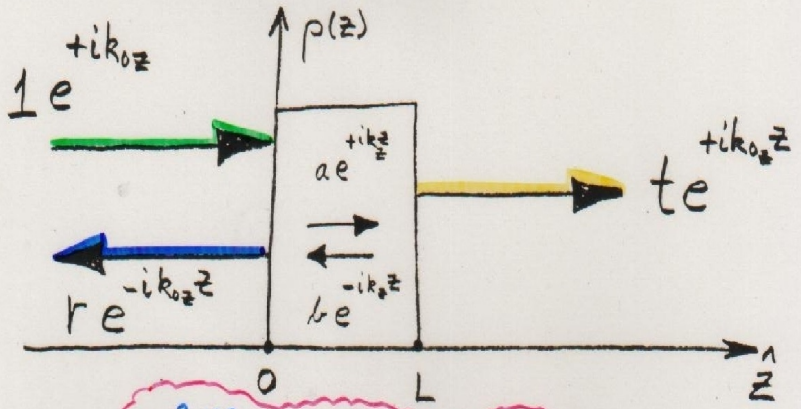

$$\frac{\partial^2 \psi(z)}{\partial z^2} + k_z^2 \psi(z) = 0$$

CONSERVATION OF MOMENTUM AND PARTICLE NUMBER REQUIRE THAT $\frac{\partial \psi(z)}{\partial z}$ AND $\psi(z)$ BE CONTINUOUS AT THE BOUNDARIES $z=0$ & $z=L$

$$\begin{pmatrix} t \\ it \end{pmatrix} e^{ik_{0z}L} = \begin{pmatrix} A & B \\ C & D \end{pmatrix} \begin{pmatrix} 1+r \\ i(1-r) \end{pmatrix}$$

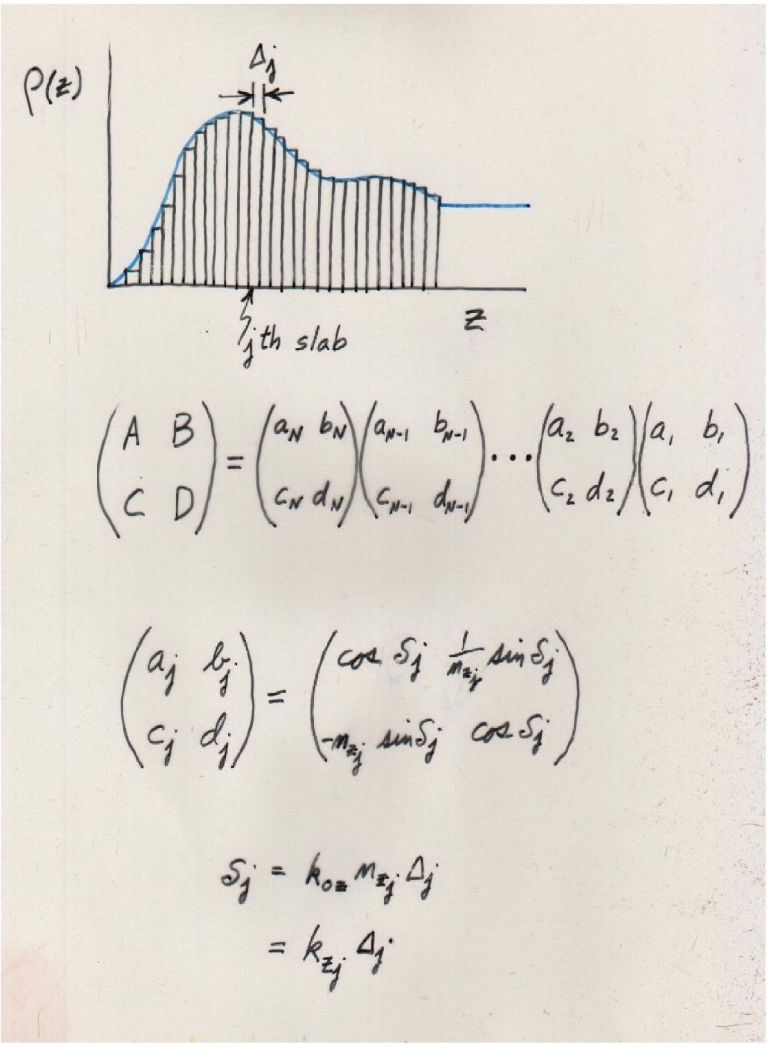

$$\begin{pmatrix} A & B \\ C & D \end{pmatrix} = \begin{pmatrix} a_N & b_N \\ c_N & d_N \end{pmatrix} \begin{pmatrix} a_{N-1} & b_{N-1} \\ c_{N-1} & d_{N-1} \end{pmatrix} \cdots \begin{pmatrix} a_2 & b_2 \\ c_2 & d_2 \end{pmatrix} \begin{pmatrix} a_1 & b_1 \\ c_1 & d_1 \end{pmatrix}$$

$$\begin{pmatrix} a_j & b_j \\ c_j & d_j \end{pmatrix} = \begin{pmatrix} \cos\delta_j & \frac{1}{m_{zj}}\sin\delta_j \\ -m_{zj}\sin\delta_j & \cos\delta_j \end{pmatrix}$$

$$\delta_j = k_{0z} m_{zj} \Delta_j$$
$$= k_{zj} \Delta_j$$

The elements A, B, C, and D of the so-called “transfer” matrix which relates the reflection, transmission, and incident wave amplitudes -- r, t, and 1, respectively -- contain all of the information about the SLD composition of the film. The transfer matrix can be constructed of a product of matrices, each of which corresponds to one successive “slice” of the film over which the SLD is taken to be a constant value. Thus, any arbitrary profile can be rendered -- and to whatever spatial resolution is needed by making the thicknesses of the slices small enough.

Part 2: Applications of NR to studies of the nanometer scale structure of thin film materials

<> Soft condensed matter:

-- polymers

-- bio-membranes

-- organic photo-voltaic films

. . .

<> Hard condensed matter:

-- magnetic materials *(to be discussed in another lecture on polarized neutrons)*

-- chemical interdiffusion (e.g., 58Ni/62Ni)

-- metal hydrides

. . .

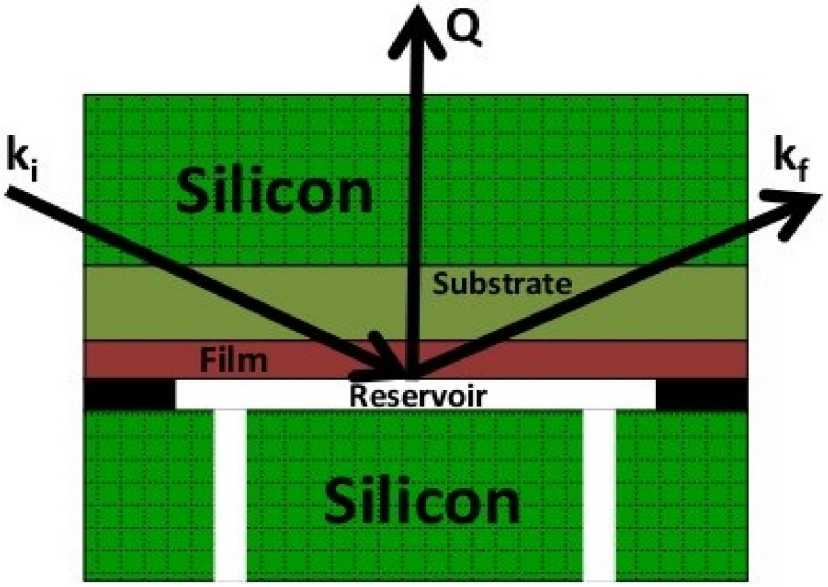

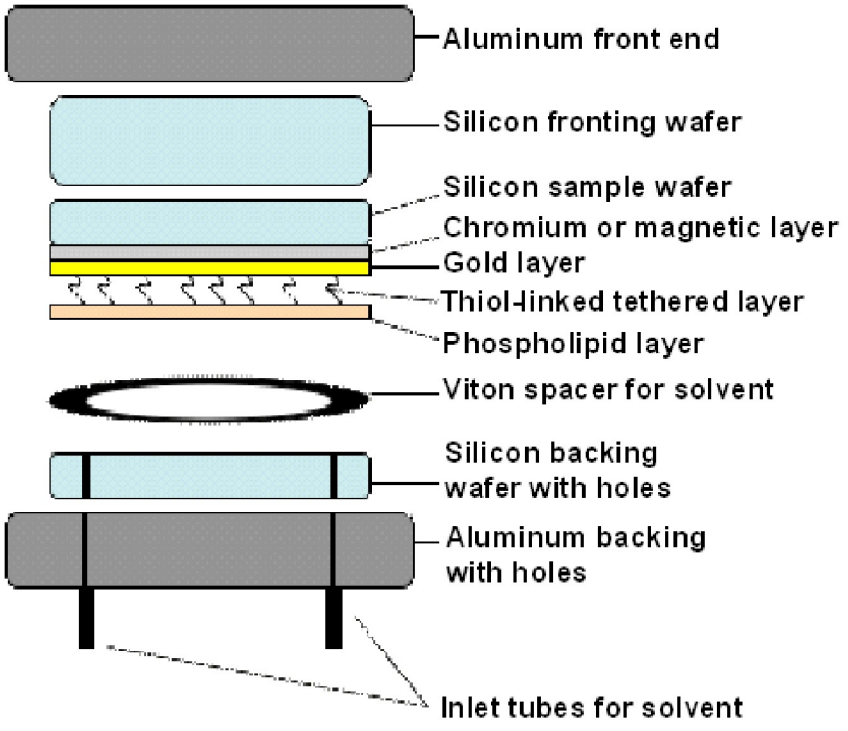

Proper design of a fluids cell is essential for optimizing the signal-to-noise ratio in neutron reflectivity measurements.

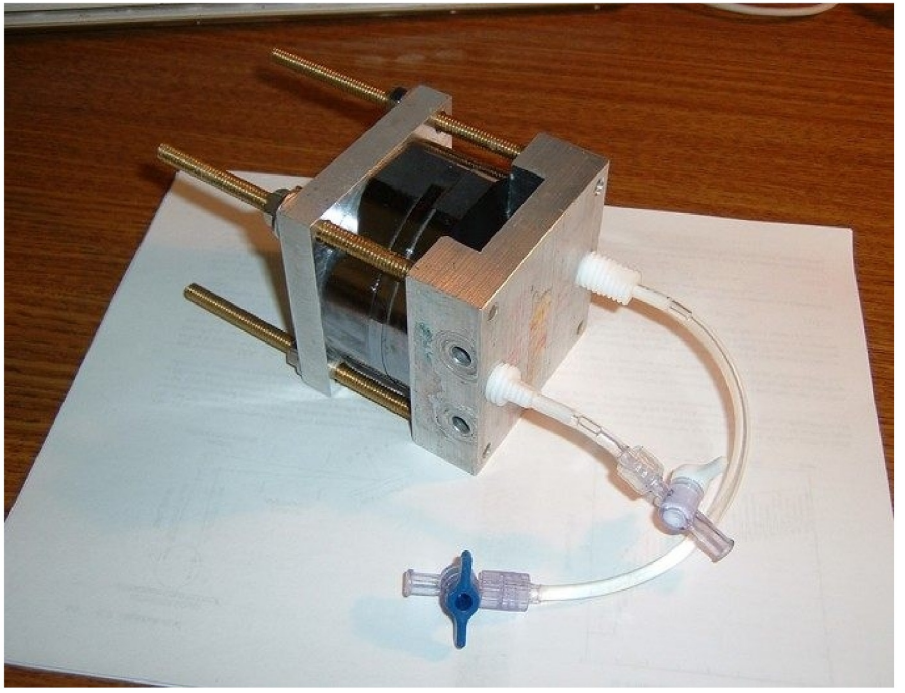

Phase Sensitive Neutron Reflectometry on a Water-Cushioned Biomembrane-Mimic

Biomimetic membranes have been developed as models of living cell membranes, and this has applications in the quest for biocompatibility of inorganic materials in biologically active mediums, such as coatings for artificial organs. A membrane consists of a lipid bilayer (two lipid layers) where hydrophobic carbon chains form the inside of the membrane and their polar head groups the interface with the aqueous surrounding medium. A supported membrane-mimic consists of a lipid-like bilayer, typically attached to a single-crystal substrate, with access to water only at the top surface [1, 2]. Here we use neutron reflectometry to study a system in which water has access to both sides of a membrane-mimic attached to such a substrate, thus making the system a closer mimic to a real cell membrane.

The system devised by Liu *et al.* [3] consists of a water-swellable polyelectrolyte that electrostatically binds to the substrate and acts as a "cushion" for the membrane, not unlike the cytoskeletal support found in actual mammalian cell membranes. The lower half of the membrane-mimic is a terpolymer that attaches to the polyelectrolyte. A phospholipid layer forms on top of the terpolymer and the bilayer is finally chemically crosslinked for added stability. The system is shown schematically in Fig. 1.

Neutron reflectivity measurements were performed at the NG-1 vertical stage reflectometer to obtain the compositional profile at every step of the assembling process of the membrane-mimic which consisted of three stages: a) polyelectrolyte multilayer (PE), b) polyelectrolyte multilayer plus terpolymer (PE+TER), and c) polyelectrolyte multilayer plus terpolymer plus phospholipid layer (PE+TER+PC) [4]. The spatial resolution attained was approximately 10 Å, about half the thickness of a membrane bilayer, making it possible to distinguish the two layers of a membrane but not the structure of a single layer.

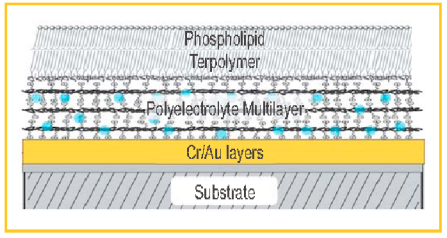

Fig. 1. Schematic diagram of a biomimetic membrane. The phospholipid layer at the top combines with the terpolymer layer to form a membrane-mimic that in turn resides on the water (blue dots) permeable "cushion" polyelectrolyte multilayer. The latter attaches electrostatically to the Au-capped substrate.

A unique compositional profile of the biomimetic film with no a priori knowledge of the sample's composition is obtained by measuring the reflectivity of equivalent samples made onto two substrates [5]. The substrates used were single crystal silicon (Si) and sapphire (Al_2O_3) coated with chromium (Cr) and then a gold (Au) layer to allow the polyelectrolytes to bind to a similar surface on both wafers.

Figure 2 shows the compositional profiles for the PE, PE+TER and PE+TER+PC assemblies in a D_2O atmosphere at 92 % relative humidity. The figure shows that the hydration of the PE layer is almost unaffected by the addition of the terpolymer and the phospholipid layer. Also, upon the addition of the phospholipid layer to the PE+TER assembly, the composite PE+TER+PC assembly shows an increase in thickness of approximately 30 Å, consistent with the formation of a single phospholipid layer at the surface. It is also clear that the addition of a phospholipid layer onto the terpolymer layer rearranges this region

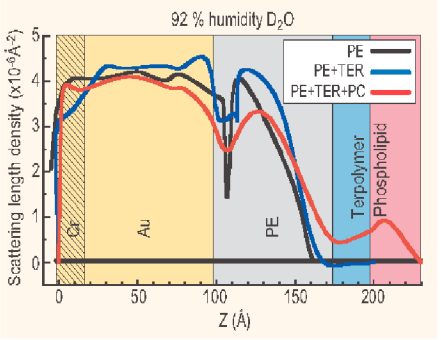

Fig. 2. Compositional profile of biomimetic membrane in a D_2O atmosphere at 92 % relative humidity at various stages of assembly on Au-capped substrate: only polyelectrolyte (PE), polyelectrolyte and terpolymer (PE+TER), polyelectrolyte, terpolymer and phospholipid (PE+TER+PC). The compositional profile is given by the scattering length density, SLD, profile when using neutrons.

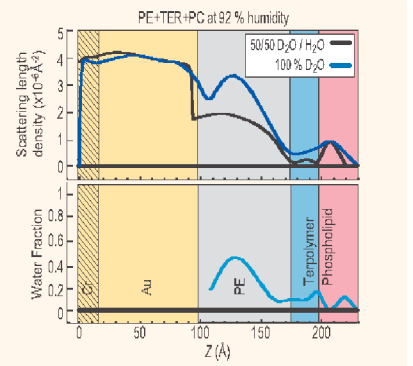

Fig. 3. Scattering length density profiles (top) and water fraction (bottom) for PE+TER+PC under indicated conditions.

significantly, since the terpolymer layer only becomes apparent after the phospholipid layer is added. It is possible to verify with an independent technique (contact angle) that the terpolymer was in fact deposited because it forms a hydrophobic outer layer. The outer surface becomes hydrophilic once the phospholipid layer is deposited onto the terpolymer layer.

Figure 3 (top) shows the profile for the PE+TER+PC assembly under 92 % relative humidity in 100 % D_2O and in 50/50 D_2O/H_2O. The overall thickness change due to the intake of water, in going from dry (not shown) to 92 % relative humidity, was found to be 20 Å. Figure 3 (bottom) shows the water fraction in the assembly under 92 % relative humidity. This is obtained by assuming that the distribution of each component in the layers is unaffected by having either D_2O or 50/50 D_2O/H_2O. From the figure it can be seen that the polyelectrolyte multilayer has a 40 % water uptake. This is a significant amount of water, which suggests that the polyelectrolyte multilayer can work as a "cushion" for membrane-mimetic systems. The terpolymer and the phospholipid layers contain an average of 10 % water, which is also significant, suggesting that these layers are not tightly packed.

The method of making equivalent samples on two substrates to obtain a unique compositional profile has a built-in congruency test, particularly useful in checking the reproducibility of the samples as well as the quality of the films. The test is to compare the calculated imaginary part of the complex reflectivity from the obtained profile with the corresponding data, as is shown in Fig. 4 for the PE+TER and PE+TER+PC assemblies. From Fig. 4 it is concluded that the PE+TER samples are homogenous and essentially identical while for the PE+TER+PC assembly, the

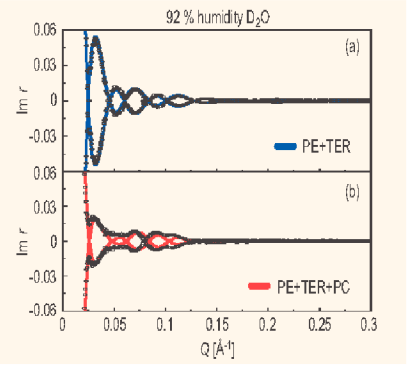

Fig. 4. Imaginary part of the complex reflectivity, Im $r(Q)$, data (symbols) and calculated curves (lines) obtained from the SLD profiles for the PE+TER and the PE+TER+PC assemblies shown in Fig. 2.

absence of true zeros, as indicated by the calculated curve, is suggestive of a small degree of sample inhomogeneity.

The system from Liu *et al.* has many characteristics desirable in a biomimetic membrane. It is a single membrane-mimic attached to a significantly hydrated soft "cushion" support that allows some membrane proteins to function. Thrombomodulin, a membrane protein relevant to blood-clotting, is being studied in this membrane-mimic environment to further develop biocompatible coatings for artificial organs [6].

References

[1] E. Sackmann, Science **271**, 43 (1996).

[2] A. L. Plant, Langmuir **15**, 5128 (1999).

[3] H. Liu, K. M. Faucher, X. L. Sun, J. Feng, T. L. Johnson, J. M. Orban, R. P. Apkarian, R. A. Dluhy, E. L. Chaikof, Langmuir **18**, 1332 (2002).

[4] U. A. Perez-Salas, K. M. Faucher, C. F. Majkrzak, N. F. Berk, S. Krueger, E. L. Chaikof, Langmuir **19**, 7688 (2003).

[5] C. F. Majkrzak, N. F. Berk, U. A. Perez-Salas Langmuir **19**, 1506 (2003).

[6] J. Feng, P. Y. Tseng, K. M. Faucher, J. M. Orban, X. L. Sun, E. L. Chaikof, Langmuir **18**, 9907 (2002).

U. A. Perez-Salas
NIST Center for Neutron Research
National Institute of Standards and Technology, Gaithersburg, MD 20899-8562

K. M. Faucher
Emory University School of Medicine, Atlanta, GA 30322

C. F. Majkrzak, N. F. Berk, S. Krueger
NIST Center for Neutron Research
National Institute of Standards and Technology
Gaithersburg, MD 20899-8562

E. L. Chaikof
Emory University School of Medicine
Atlanta, GA 30322

The next series of slides shows a NR study of the location of water within a particular biomimetic membrane of interest to a vascular surgeon (who is attempting to develop synthetic replacements for arteries and veins in medical applications). Such synthetic vessels must have bio-compatible coatings which won't foster an immune system response.

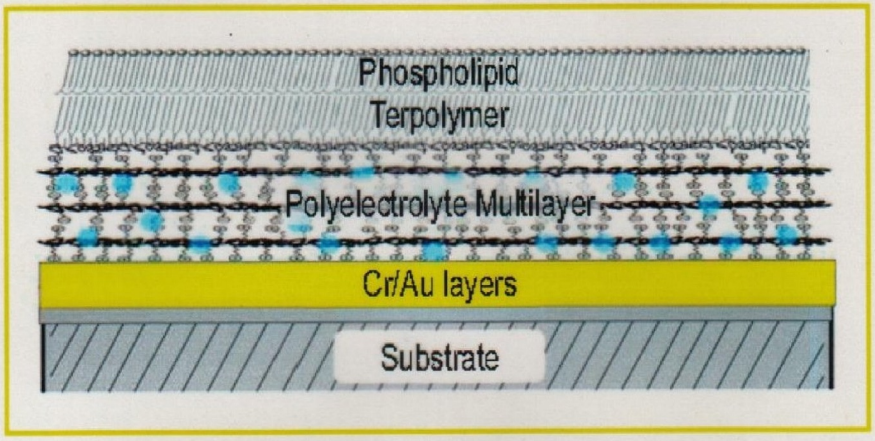

Fig. 1. Schematic diagram of a biomimetic membrane. The phospholipid layer at the top combines with the terpolymer layer to form a membrane-mimic that in turn resides on the water (blue dots) permeable "cushion" polyelectrolyte multilayer. The latter attaches electrostatically to the Au-capped substrate.

(Work of Ursula Perez-Salas, K. Faucher, E. Chaikof, et al.)

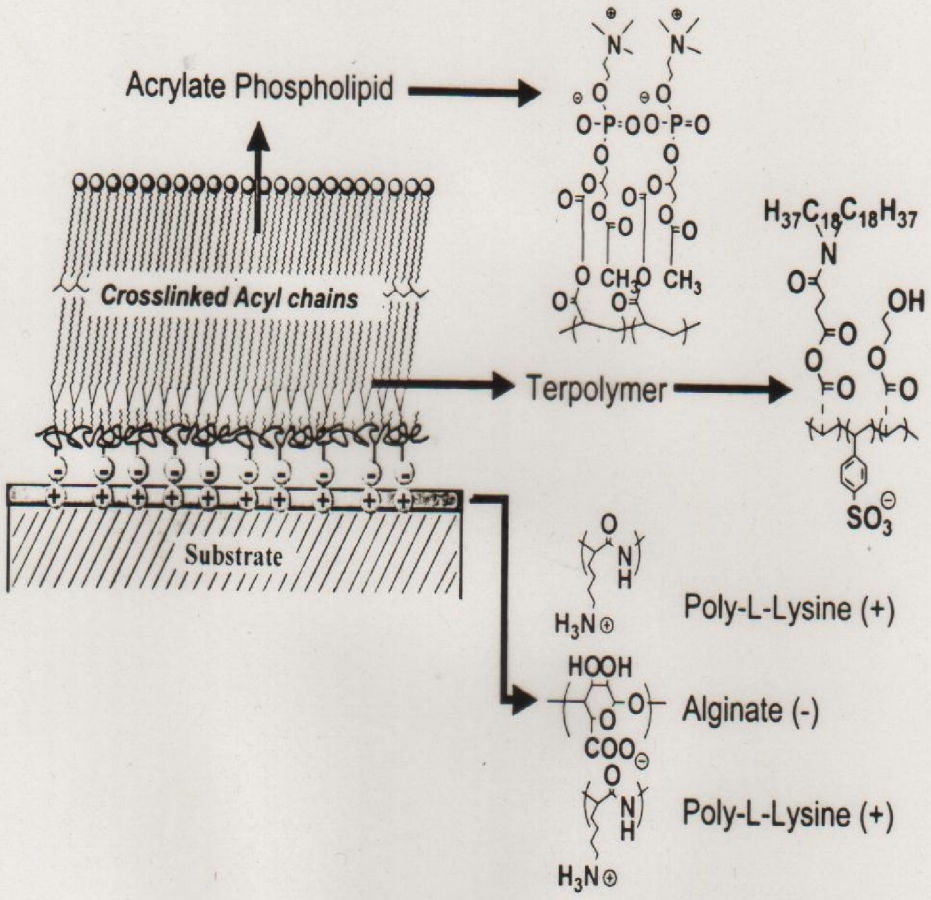

Figure 1:

1 Schematic representation the terpolymer (TER)-acrylate phospholipid (PC) membrane mimic supported on a polyelectrolyte multilayer(PE) "cushion". . . . . .

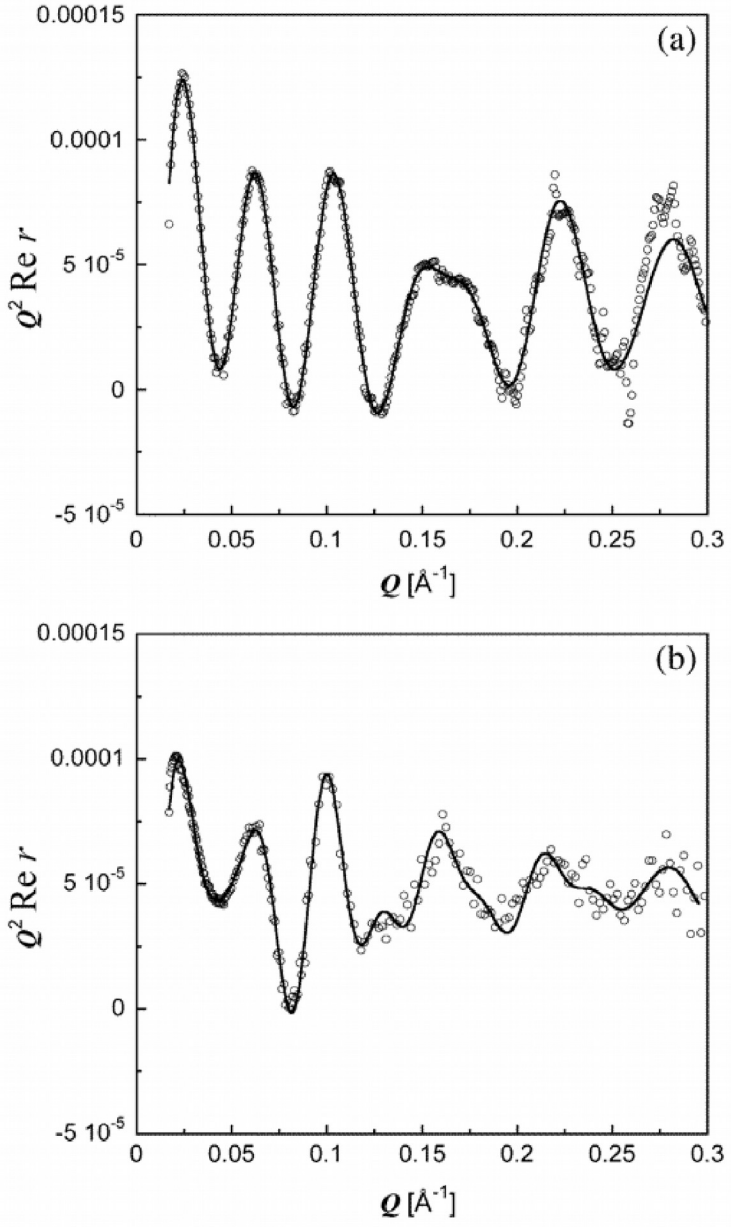

Typical real parts of reflection amplitudes obtained via phase-senistive neutron reflectometry methods for the biomimetic film structure presented in the previous slides.

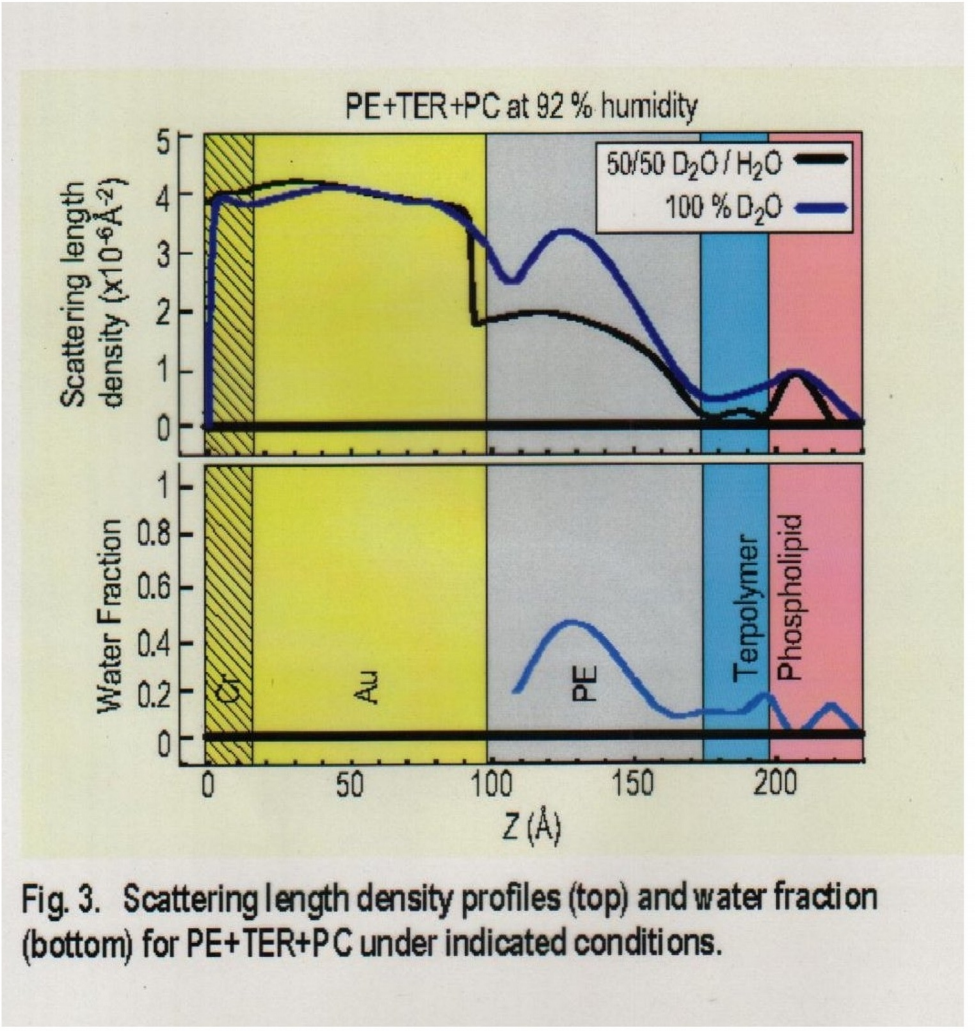

Fig. 3. Scattering length density profiles (top) and water fraction (bottom) for PE+TER+PC under indicated conditions.

After a number of different reflectivity measurements with various aqueous reservoir contrast values for H2O / D2O ratios, it was possible to deduce, from the analysis of that data, the water distribution across the thickness of the film structure. As shown in the figure above, the water is found to reside primarily within the poly-electrolyte layer.

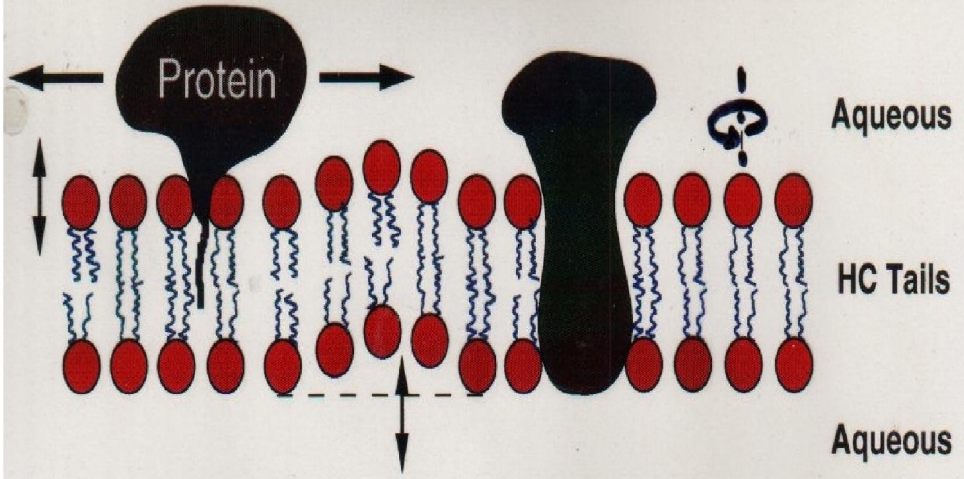

Supported Lipid Bilayers

A model system to mimic the structure and dynamics of cell membranes.

Proteins in Lipid Bilayers

- Difficult to characterize by traditional x-ray crystallography.
- Play a crucial role in cell function
  - regulate ion and nutrient transport
  - engage in binding, signalling and cell recognition
  - participate in cell fusion events.

Biosensors (Anne Plant & coworkers)

Melittin in Hybrid Bilayer Membranes

S. Krueger, A. Plant, et al., NIST (Langmuir)

- pore-forming toxin
- used as model membrane peptide
- active in HBMs

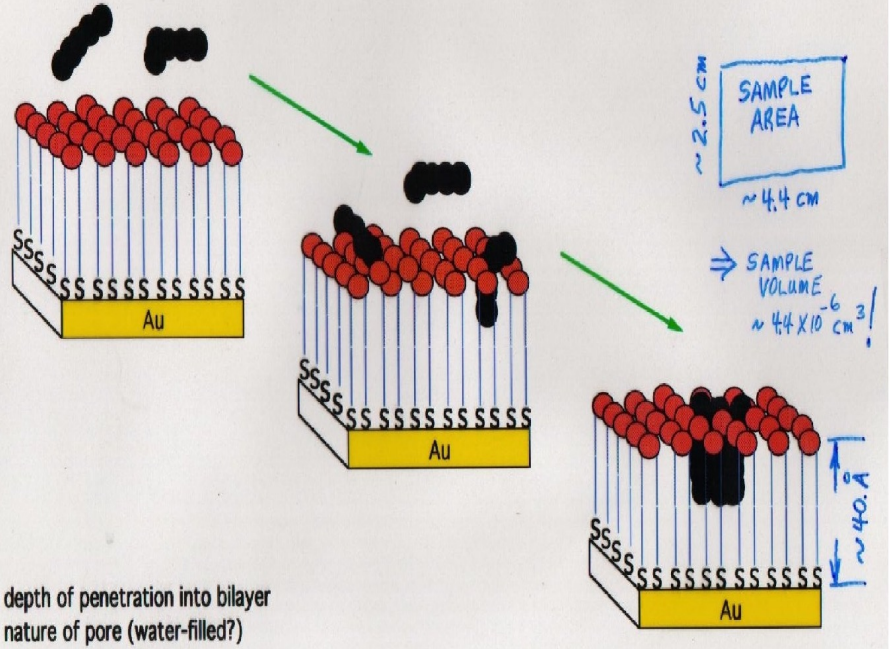

- depth of penetration into bilayer
- nature of pore (water-filled?)
- conformational changes
- random or ordered distribution?
- influence on surrounding lipids (location,conformation)

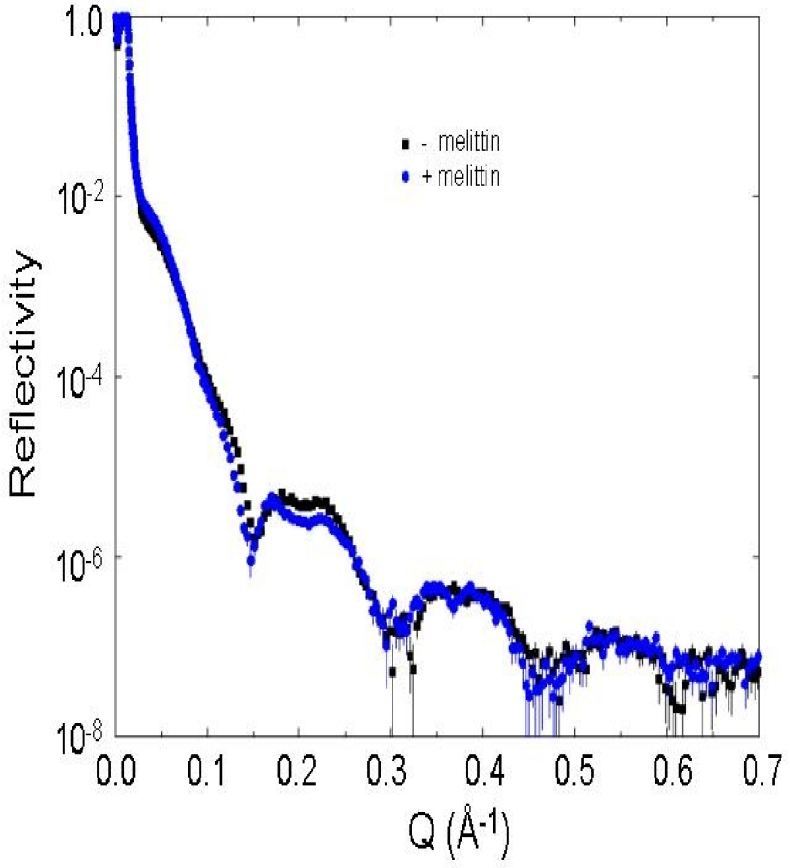

Specular neutron reflectivity data sets collected from a lipid bilayer membrane with and without exposure to melittin. Even on this log scale, significant differences are observable all across the reflectivity curves. Measurements of the reflectivity were obtained over nearly eight orders of magnitude and out to a Q of 0.72 inverse Angstroms -- which corresponds to a real space resolution of a fraction of a nano-meter in the SLD depth profile.

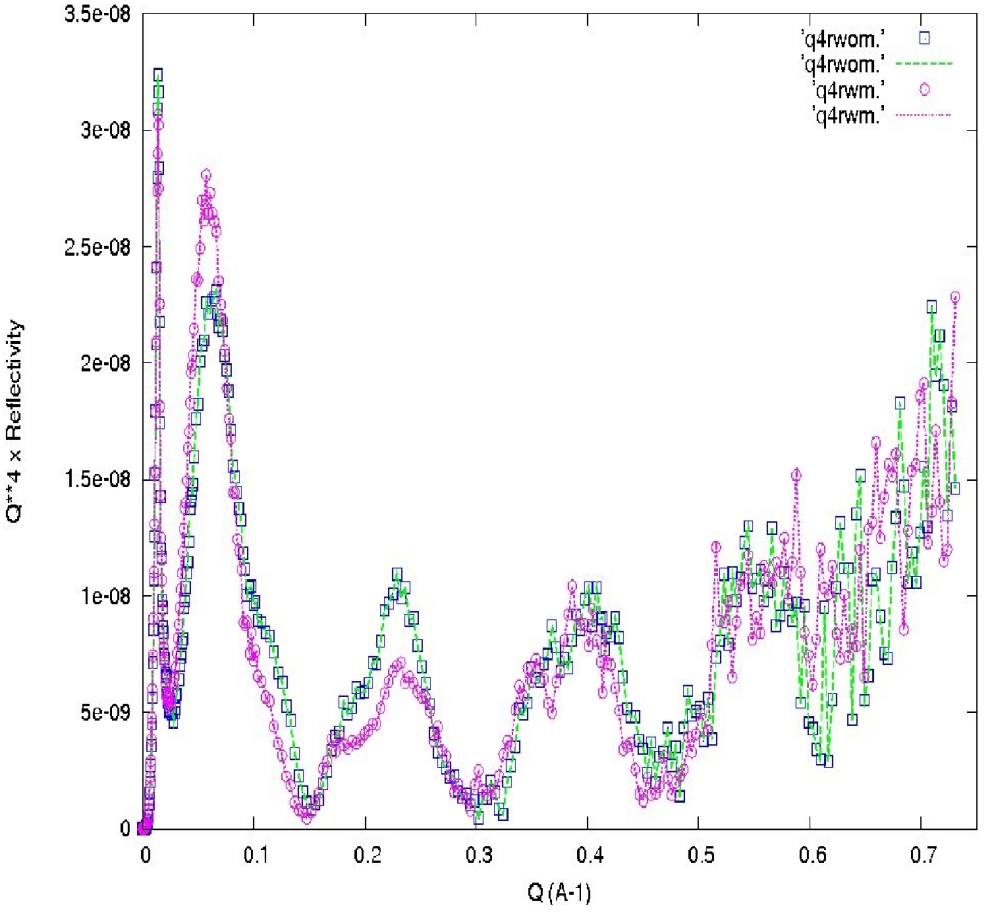

Multiplying the reflectitivities of the previous slide by Q^4 enhances the differences between the data obtained with and without melittin.

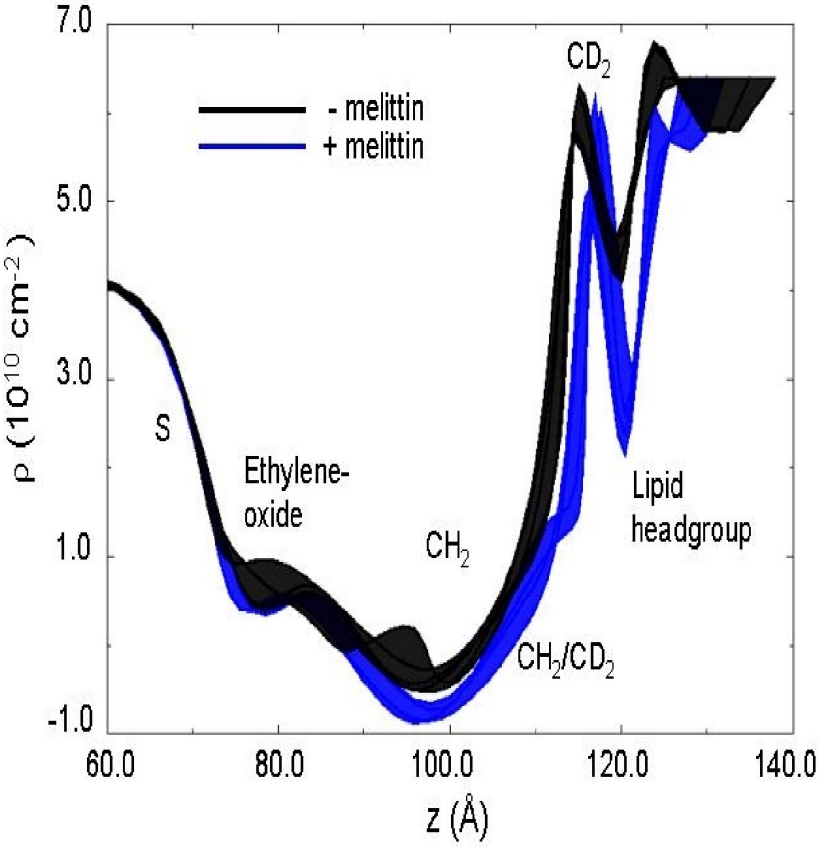

The scattering length density profiles obtained from fitting the reflectivity data -- the thickness of the plotted lines are a measure of the uncertainty in the SLD values. The data suggest that the melittin molecules perturb the outer leaflet of the bilayer membrane but do not penetrate significantly deeper.

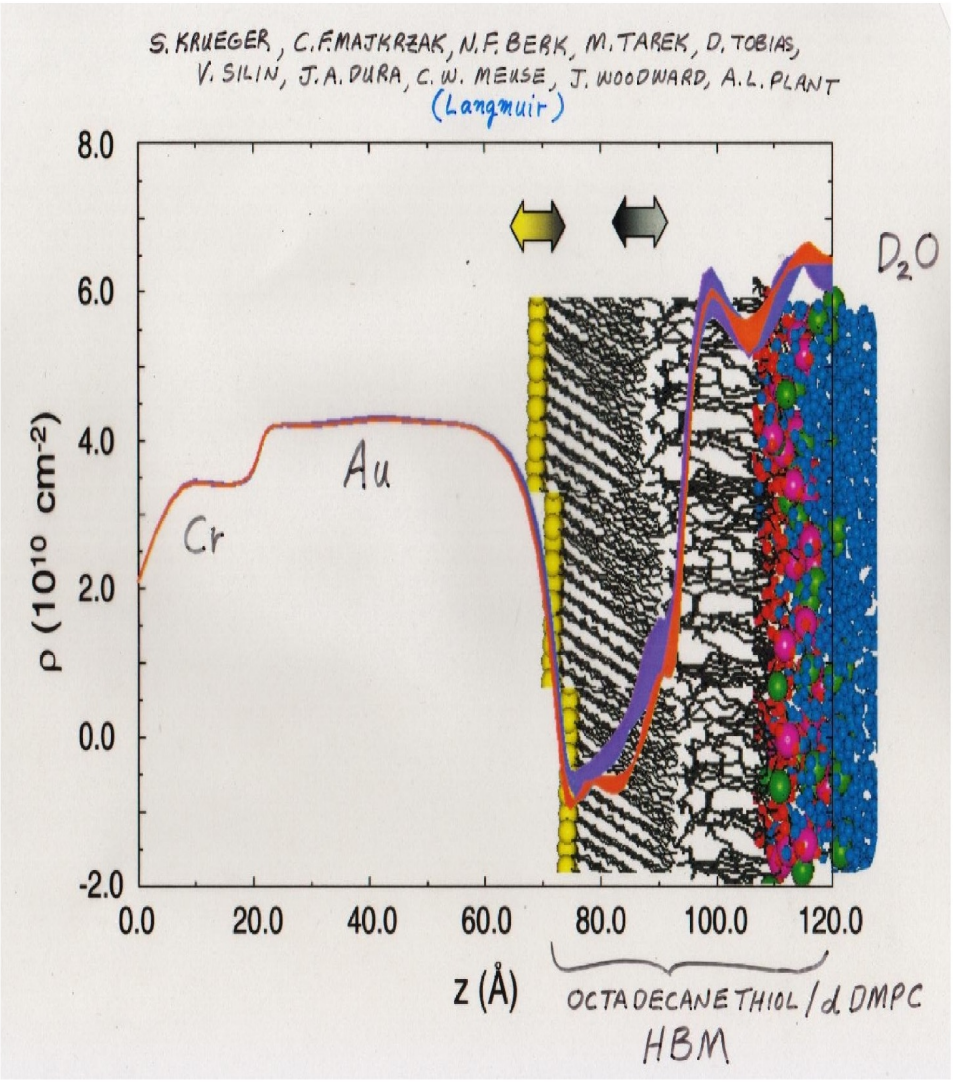

Comparison of the SLD profile for the lipid bilayer (without melittin) as obtained from the specular neutron reflectivity measurement with that predicted by a molecular dynamics simulation.

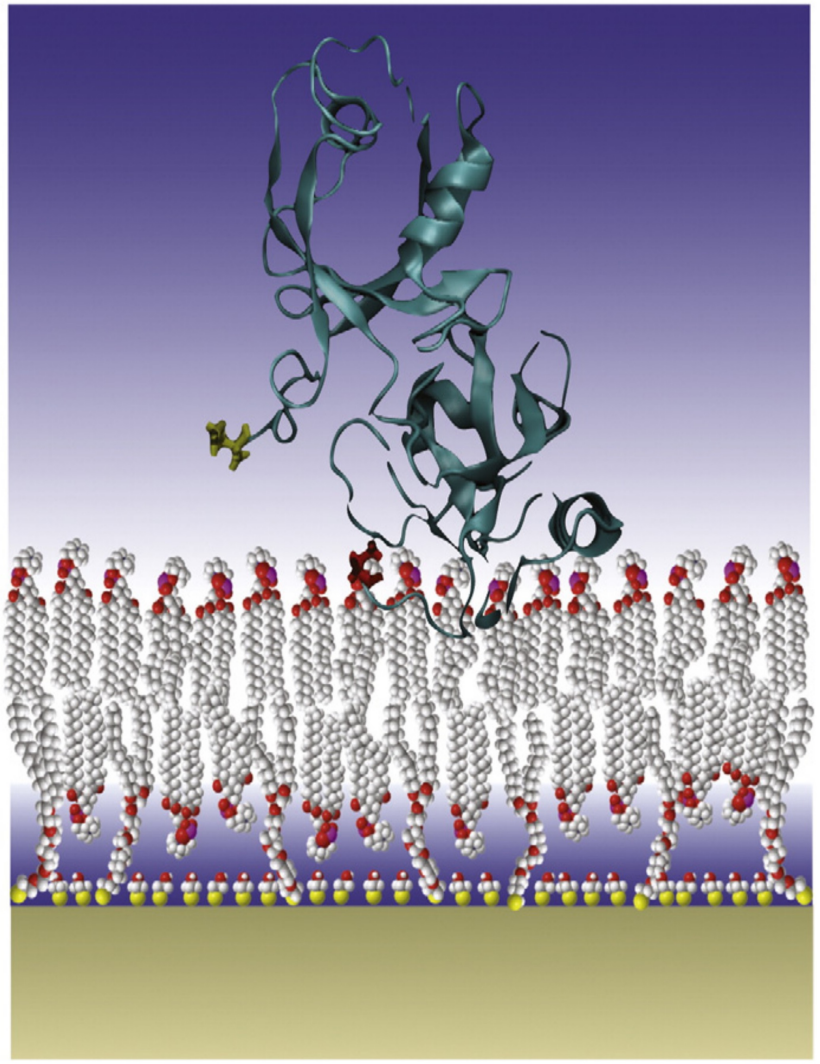

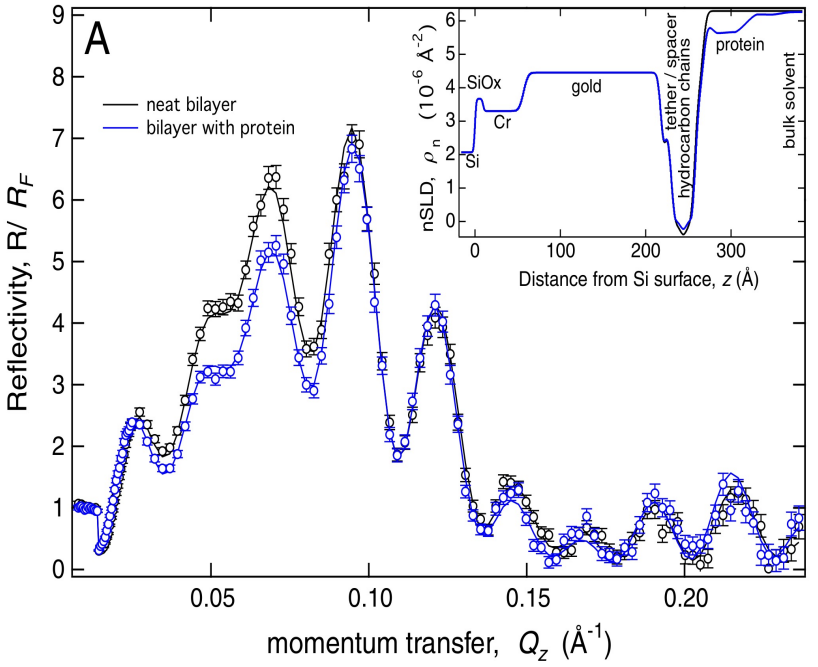

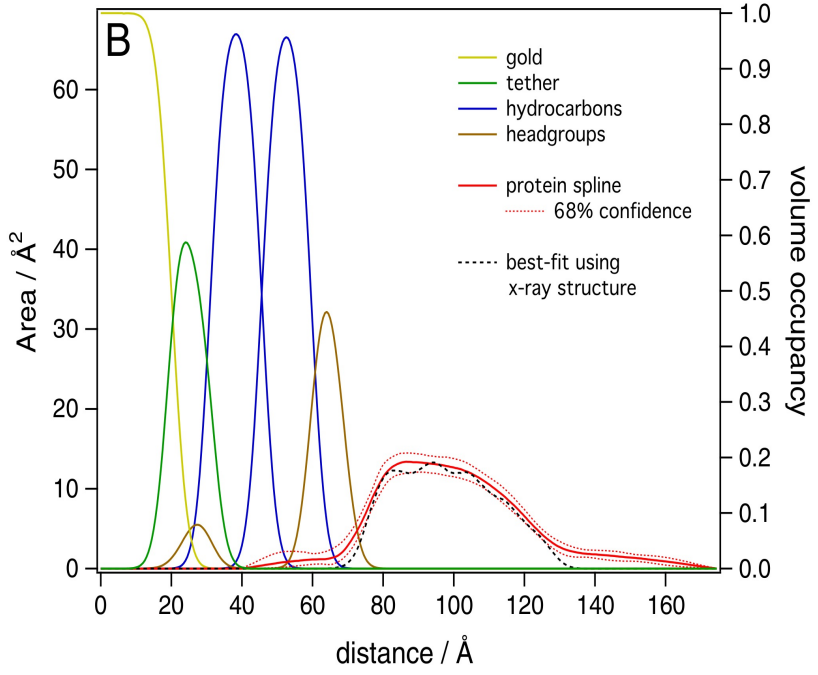

Fig. 1. Cartoon of a sparsely tethered bilayer lipid membrane (stBLM). Following the formation of a self-assembled monolayer of PEGylated lipidic tether molecules, grafted to a gold surface via thiol bonds, the bilayer is completed using either vesicle fusion or rapid solvent exchange. Sparse grafting of tethers is achieved by co-adsorption with βME. This sketch also shows the structure of a membrane-associated protein, GRASP55, whose orientation and membrane penetration have been determined with neutron reflectometry [19].

A sampling (on this and the next slide) of more recent specular NR studies of compositional depth pofiles of biological macro-molecules attached to or embedded in lipid bilayer membranes. These results are remarkable -- if not spectacular (at least in my opinion)!

Water-soluble membrane-associated proteins

>50% of biological NR beam time for biomedical applications using tBLMs

Active projects (last 2 cycles):

- Dengue
- Gaucher's disease
- GRASP
- HIV Gag & antibodies
- RSV & MLV
- Neurotransmitter
- OmpA/LA
- Parkinson's disease
- PTEN Tumor surpressor
- T-Cell receptor

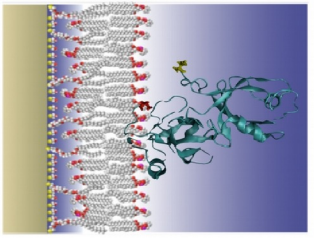

GRASP orientation at a tethered bilayer lipid membrane (tBLM) as determined by NR

Collaborative staff involvement:

- experimental planning
- substrate preparation
- tether synthesis
- neutron measurement
- data analysis

Bulent Akgun, Frank Heinrich, Mathias Lösche, Duncan McGillivray, Hirsh Nanda, David Vanderah

Typical reflectometry data for tBLM experiments

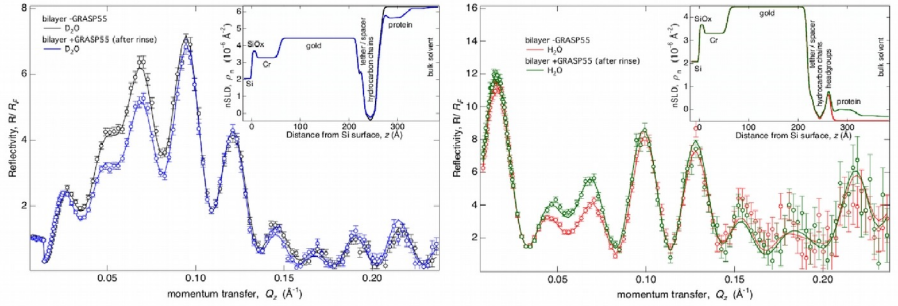

NR data measured on NG7, and best-fits for GRASP association with lipid membranes, project with A. Linstedt, University of Pittsburgh

Bulent Akgun, Frank Heinrich, Mathias Lösche, Duncan McGillivray, Hirsh Nanda

Example: Dengue Virus Envelope Protein

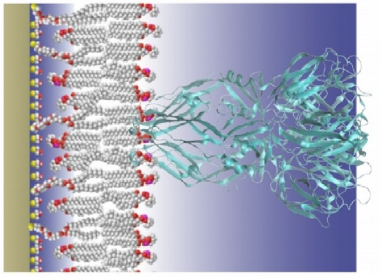

Visualization. Project with Mike Kent, Sandia National Labs.

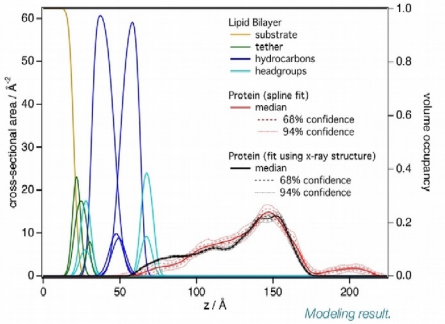

Modeling result.

- Monte-Carlo Markov Chain uncertainty analysis
- Composition-space modeling of the bilayer
- Free-form fitting of structurally unknown components of the architecture
- Usage of PDB structure files for position and orientation of rigid proteins

Bulent Akgun, Frank Heinrich, Paul Kienzle, Sushil Satija

www.ncnr.nist.gov/programs/reflect/

Combining NR with Molecular Simulations

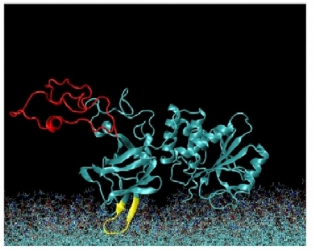

MD simulation snapshot of PTEN tumor suppressor association with a PS-containing lipid membrane

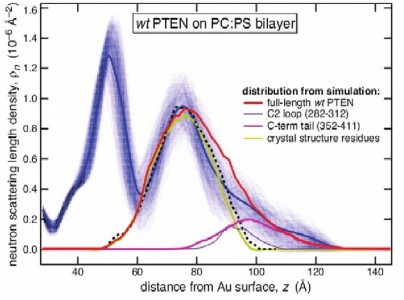

Comparison of MD and NR results, Shenoy, S. et al.. J. Struct. Biol. 1–15 (2012).

Comparison of experimental data with results from:

- MD simulation
- Monte Carlo conformational search (SASSIE) results

Future Challenges:

- Ensemble averaging, integrating NR and simulation

Joseph Curtis, Mathias Lösche, Hirsh Nanda

$$\Psi = \psi_+ + \psi_- = \underbrace{C_{0_+} e^{i\vec{k}_+\cdot\vec{r}} \begin{pmatrix} 1 \\ 0 \end{pmatrix}}_{C_+} + \underbrace{C_{0_-} e^{i\vec{k}_-\cdot\vec{r}} \begin{pmatrix} 0 \\ 1 \end{pmatrix}}_{C_-}$$

$$k_\pm = n_\pm k_0$$

$$n_\pm^2 = 1 - \frac{2m}{(\hbar k_0)^2}\left(V_N \pm \mu B\right)$$

$$= 1 - \frac{4\pi}{k_0^2}\left(\rho_N \pm \rho_M\right)$$

NUCLEAR SLD

MAGNETIC SLD

$$|\Psi|^2 = \Psi^{*T}\Psi = \begin{pmatrix} \psi_+^* & \psi_-^* \end{pmatrix}\begin{pmatrix} \psi_+ \\ \psi_- \end{pmatrix}$$

$$= \psi_+^*\psi_+ + \psi_-^*\psi_-$$

$$= C_{0_+}^* e^{-i\vec{k}_+\cdot\vec{r}}\, C_{0_+} e^{+i\vec{k}_+\cdot\vec{r}} + C_{0_-}^* e^{-i\vec{k}_-\cdot\vec{r}}\, C_{0_-} e^{+i\vec{k}_-\cdot\vec{r}}$$

$$= |C_{0_+}|^2 + |C_{0_-}|^2 = 1$$

The neutron is a spin-half quantum object and possesses a corresponding magnetic moment. Its wave function must therefore be described as a "spinor" which is composed of two terms, each representing one of two possible spin "eigenstates". In a magnetic field, the energies associated these two eigenstates are different. This can have significant consequences for the interaction of the neutron with magnetic fields and materials.

So our description of a neutron gets a bit more complicated when we have to take into account its spin and moment. But, as I hope you will see, that added complexity makes the neutron a more sensitive and useful probe of matter, even that which is not itself magnetic.

The magnetic SLD is a product of the number of magnetic atoms per unit volume times their characteristic magnetic scattering length (usually designated "p") -- *or* is proportional to a macroscopic magnetic induction field "B".

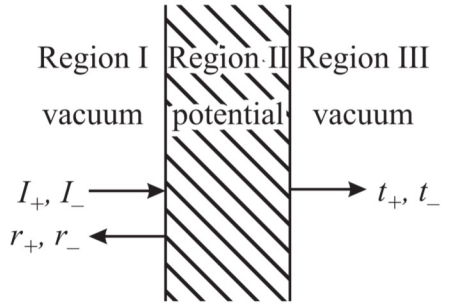

Figure 1.12: Schematic depiction of specular neutron reflection for polarized beams.

$$\begin{aligned}\left[-\frac{\hbar^2}{2m}\frac{\partial^2}{\partial z^2}+V_{++}(z)-E\right]\psi_+(z)+V_{+-}(z)\psi_-(z) &= 0 \qquad (1.56)\\ \left[-\frac{\hbar^2}{2m}\frac{\partial^2}{\partial z^2}+V_{--}(z)-E\right]\psi_-(z)+V_{-+}(z)\psi_+(z) &= 0\end{aligned}$$

where, as in the nonmagnetic case, the total energy E of the neutron is conserved so that there is no explicit time dependence. In matrix notation we can write Equation 1.56 as

$$\left[-\frac{\hbar^2}{2m}\frac{\partial^2}{\partial z^2}\begin{pmatrix}1&0\\0&1\end{pmatrix}+\begin{pmatrix}V_{++}(z)&V_{+-}(z)\\V_{-+}(z)&V_{--}(z)\end{pmatrix}-E\begin{pmatrix}1&0\\0&1\end{pmatrix}\right]\begin{pmatrix}\psi_+\\\psi_-\end{pmatrix}=0 \qquad (1.57)$$

where the net potential operator $\check{V}=\check{V}_{\rm N}+\check{V}_{\rm M}$ has a magnetic contribution $\check{V}_{\rm M}$ written in terms of the Pauli matrices of Equation 1.38 as

$$\begin{aligned}\check{V}_{\rm M} &= \check{\mu}\cdot\vec{B}=-\mu\check{\sigma}\cdot\vec{B}=-\mu\left(\check{\sigma}_x B_x+\check{\sigma}_y B_y+\check{\sigma}_z B_z\right)\\ &= -\mu\left[\begin{pmatrix}0&1\\1&0\end{pmatrix}B_x+\begin{pmatrix}0&-\mathrm{i}\\\mathrm{i}&0\end{pmatrix}B_y+\begin{pmatrix}1&0\\0&-1\end{pmatrix}B_z\right] \qquad (1.58)\\ &= -\mu\begin{pmatrix}B_z&B_x-\mathrm{i}B_y\\B_x+\mathrm{i}B_y&B_z\end{pmatrix}.\end{aligned}$$

For polarized neutrons, solving the Schroedinger equation of motion -- say for specular reflection, as we have done previously in the absence of magnetic fields -- now requires a simultaneous solution of a pair of coupled equations. This takes into account the possibility that a scattering event or interaction will involve a change in the neutron's spin eigenstate from “+” or “up” to “-” or “down” (or not). Note that the nuclear and magnetic SLDs or potentials are additive and thus result in an interference in some cases that is neutron spin-dependent.

The potential energy or SLD can no longer be described as a scalar quantity but is, instead, represented by matrix -- the neutron moment itself is a vector operator composed of 2 x 2 so-called “Pauli” matrices.

$$\check{V}_{\mathrm{N}} = \frac{2\pi\hbar^2}{m}\begin{pmatrix} Nb & 0 \\ 0 & Nb \end{pmatrix} = \frac{2\pi\hbar^2}{m}\begin{pmatrix} \rho_{\mathrm{N}} & 0 \\ 0 & \rho_{\mathrm{N}} \end{pmatrix} \qquad (1.59)$$

$$\check{V}_{\mathrm{M}} = \frac{2\pi\hbar^2}{m}\begin{pmatrix} Np_z & Np_x - \mathrm{i}Np_y \\ Np_x + \mathrm{i}Np_y & -Np_z \end{pmatrix} \qquad (1.60)$$

$$\check{V} = \frac{2\pi\hbar^2}{m}\begin{pmatrix} Nb + Np_z & Np_x - \mathrm{i}Np_y \\ Np_x + \mathrm{i}Np_y & Nb - Np_z \end{pmatrix} = \frac{2\pi\hbar^2}{m}\begin{pmatrix} \rho_{++} & \rho_{+-} \\ \rho_{-+} & \rho_{--} \end{pmatrix}. \qquad (1.61)$$

Setting $E = \hbar^2 k_0^2/(2m)$, the coupled equations of motion 1.56 can be rewritten in a form analogous to Equation 1.15 for the nonmagnetic case:

$$\begin{aligned} \left[\frac{\partial^2}{\partial z^2} + \frac{Q^2}{4} - 4\pi\rho_{++}(z)\right]\psi_+(z) - 4\pi\rho_{+-}(z)\psi_-(z) &= 0 \qquad (1.62) \\ \left[\frac{\partial^2}{\partial z^2} + \frac{Q^2}{4} - 4\pi\rho_{--}(z)\right]\psi_-(z) - 4\pi\rho_{-+}(z)\psi_+(z) &= 0 \end{aligned}$$

where we have substituted $Q = 2k_{0z}$.

At the end of the day, we can arrive at a similar, but somewhat more complicated, relationship between transmitted (T_+, T_-), reflected (R_+, R_-), and incident (I_+, I_-) wave amplitudes which are now spin-dependent. Just as we did for the non-polarized case, any arbitrary SLD profile can be rendered into slices of constant SLD (the "sliced-bread" analogy) for piece-wise continuous solution by imposing the boundary conditions of continuity on the wave function and its first derivative at each interface.

$$\begin{pmatrix} t_+ \\ t_- \\ \frac{\mathrm{i}Q}{2}t_+ \\ \frac{\mathrm{i}Q}{2}t_- \end{pmatrix} = \prod_{l=N}^{1}\begin{pmatrix} A_{11} & A_{12} & A_{13} & A_{14} \\ A_{21} & A_{22} & A_{23} & A_{24} \\ A_{31} & A_{32} & A_{33} & A_{34} \\ A_{41} & A_{42} & A_{43} & A_{44} \end{pmatrix}_l \begin{pmatrix} I_+ + r_+ \\ I_- + r_- \\ \frac{\mathrm{i}Q}{2}(I_+ - r_+) \\ \frac{\mathrm{i}Q}{2}(I_- - r_-) \end{pmatrix} \qquad (1.109)$$

where

$$\prod_{l=N}^{1}\check{A}_l = \check{A}_N\check{A}_{N-1}\cdots\check{A}_l\cdots\check{A}_2\check{A}_1. \qquad (1.110)$$

Polarized Beam Reflectometer (PBR) at NIST

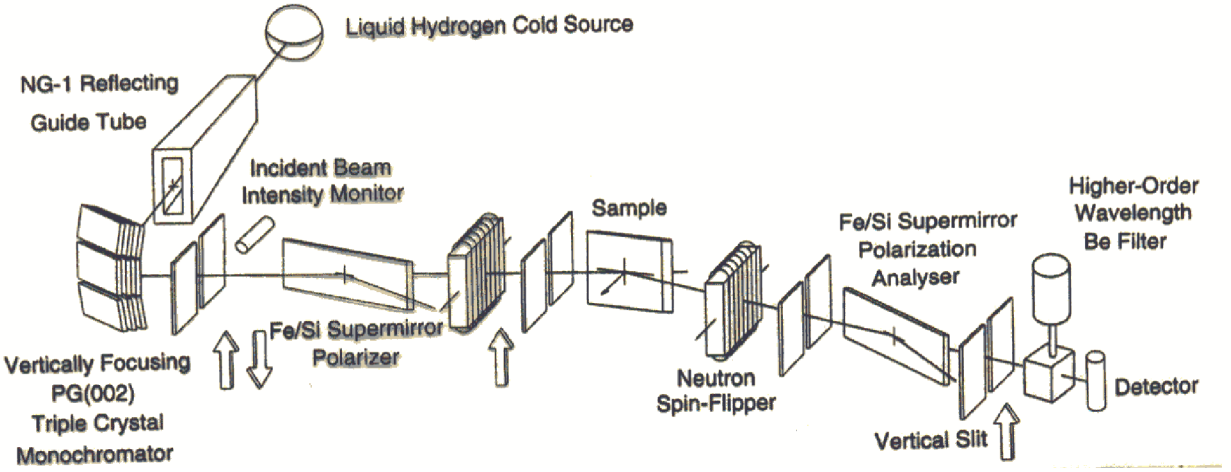

$$F^{\pm\pm} \propto \sum_{j=1}^{N} \left[b_{s_j} \pm P_{s_j} \cos\phi_j \right] e^{iQu_j}$$

$$F^{\pm\mp} \propto \sum_{j=1}^{N} P_{s_j} \sin\phi_j \, e^{iQu_j}$$

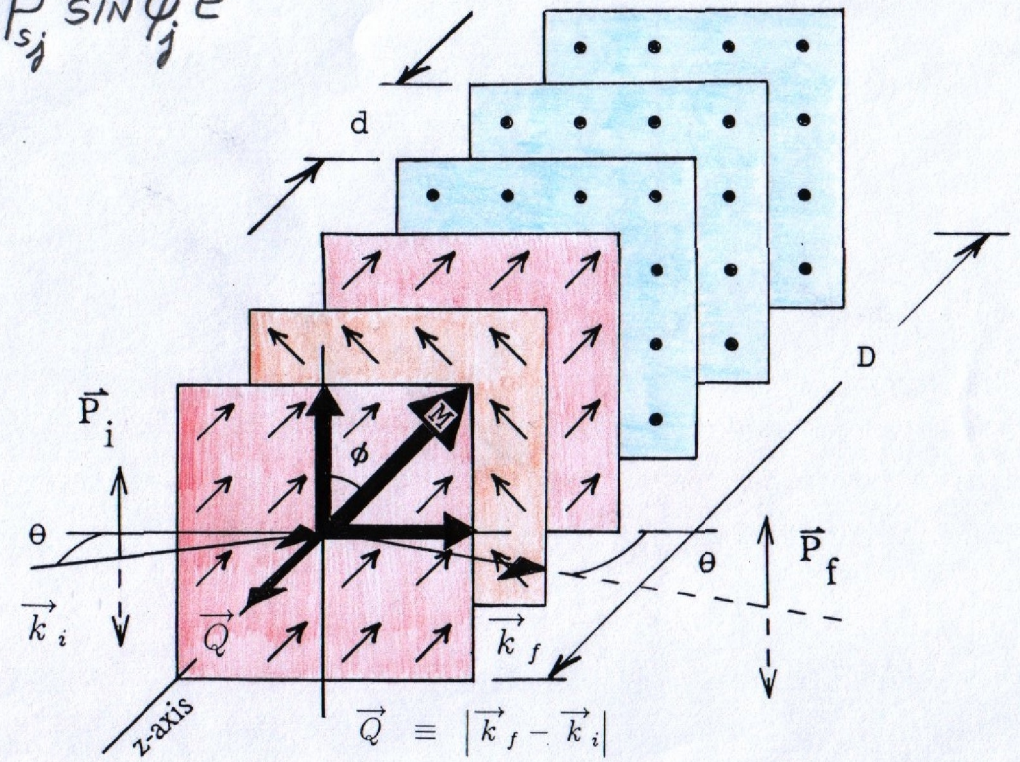

The above diagram illustrates a particularly useful configuration resulting in the ability to determine not only the magnitude of the net magnetization in each of the successive planes in a layered material, but also the direction of that magnetic moment.

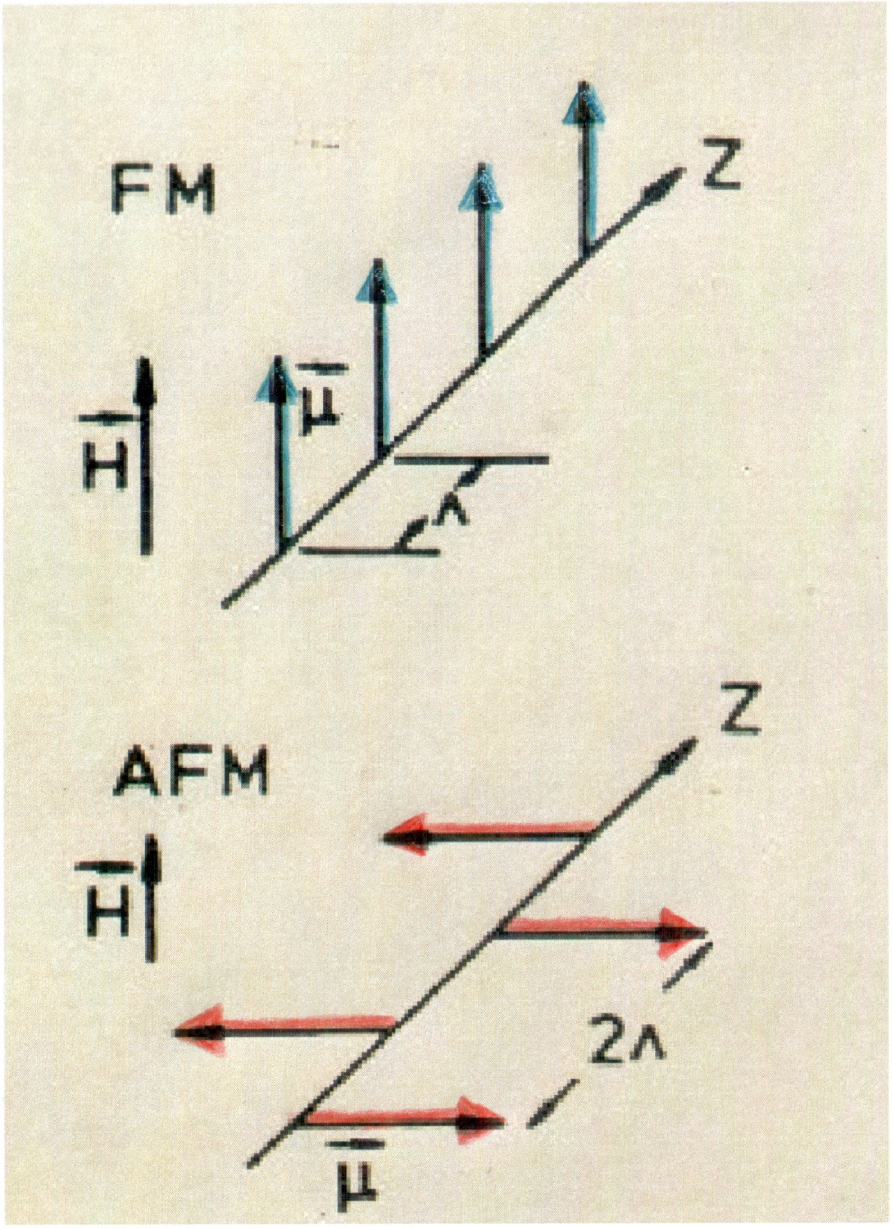

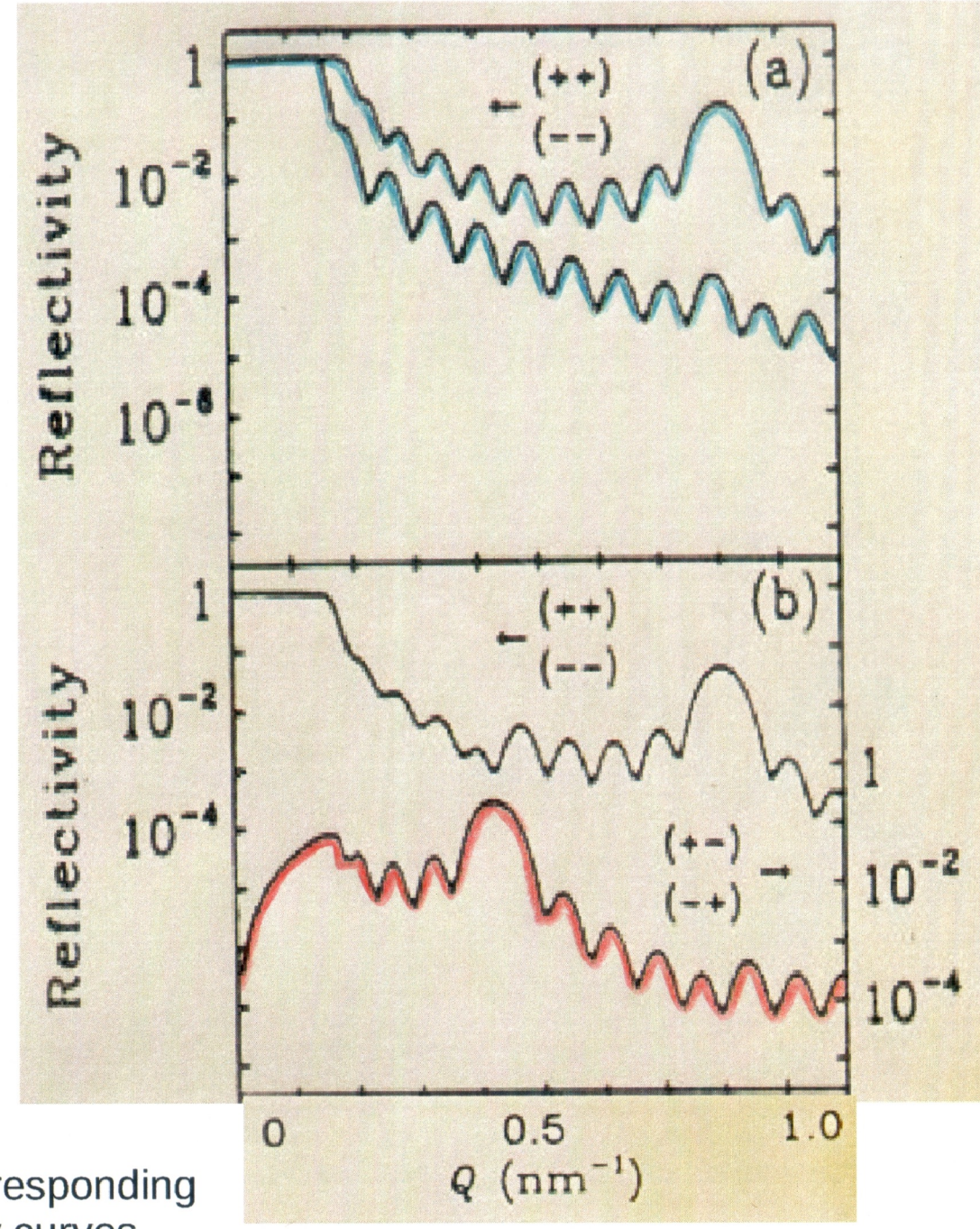

Two basic magnetic structures and their corresponding spin-dependent polarized neutron reflectivity curves (after Ankner, Schreyer, Majkrzak, and Zabel).

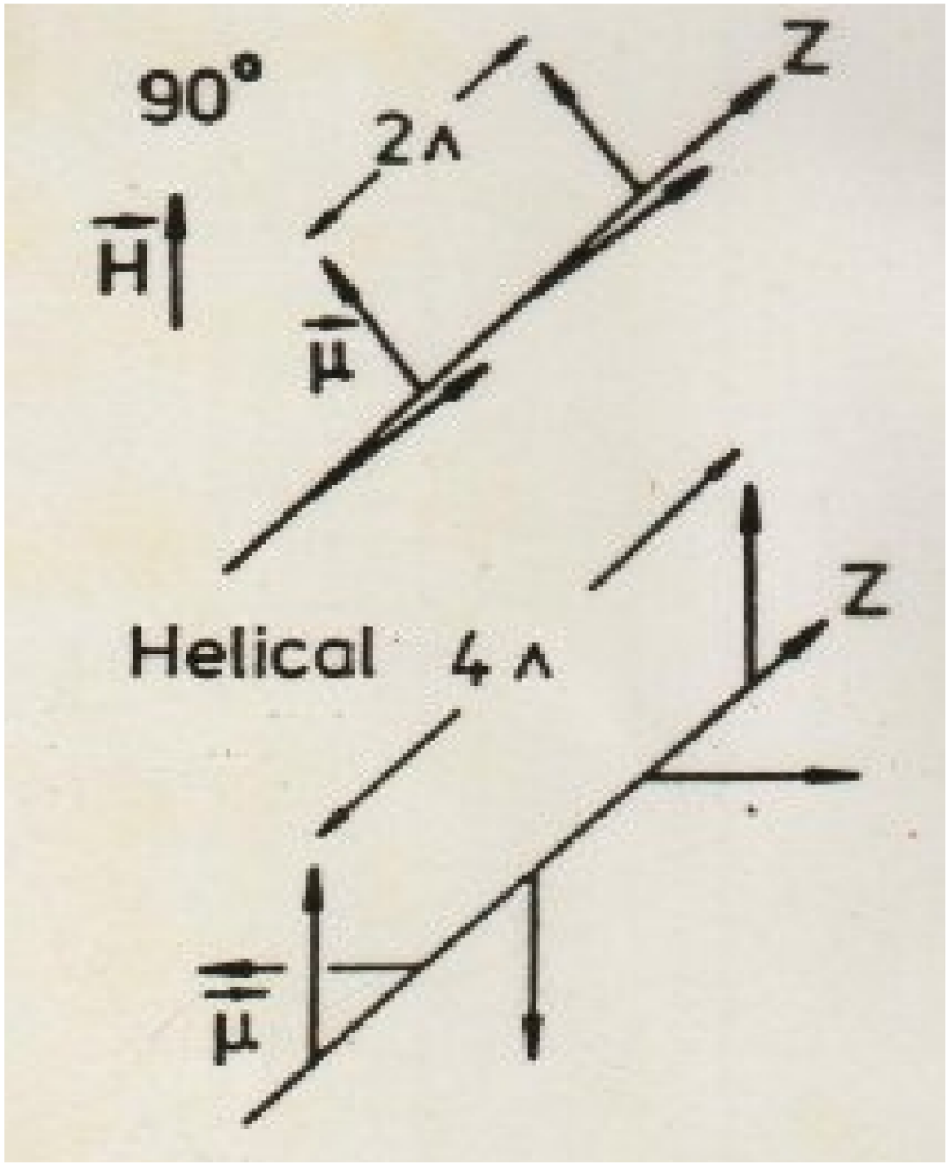

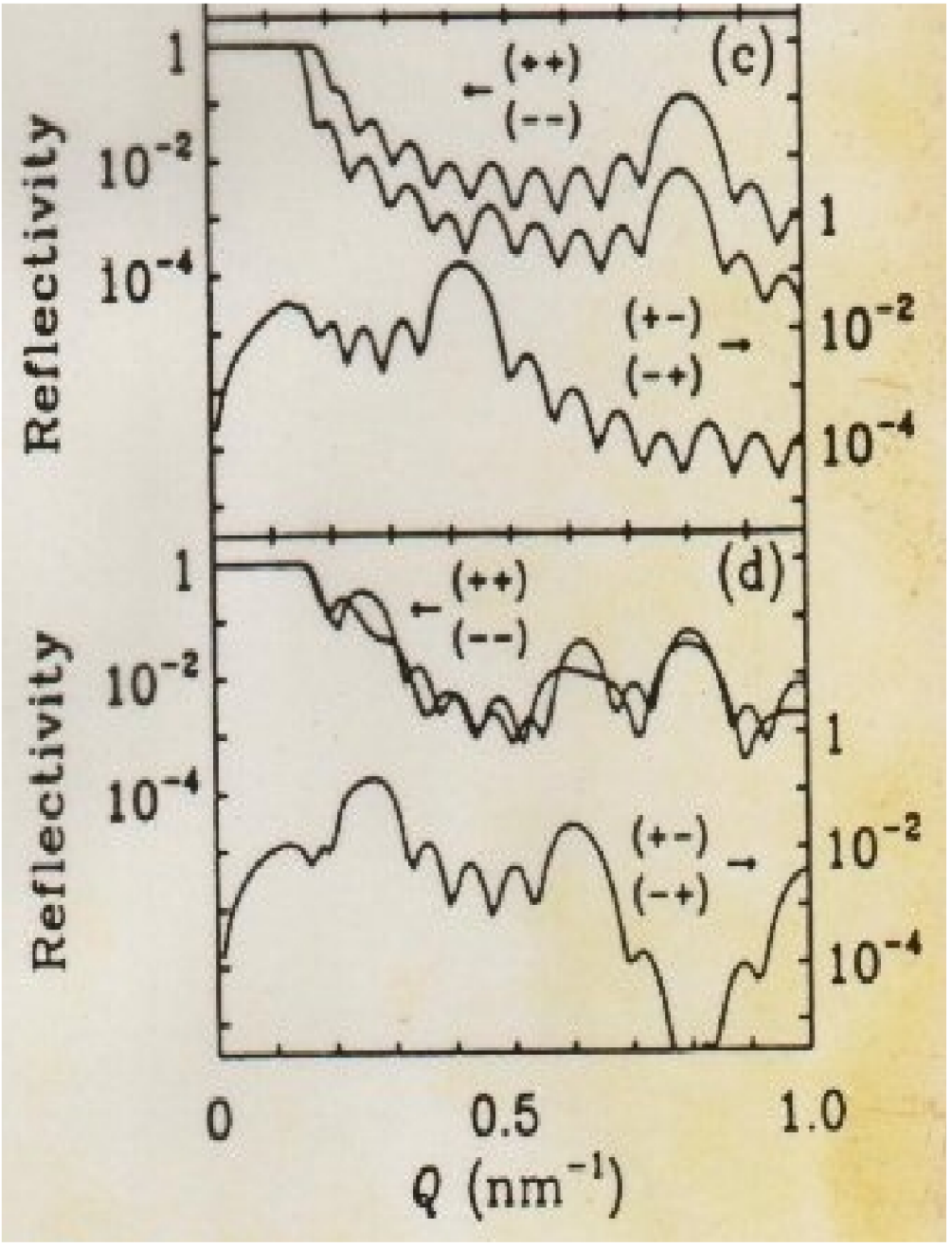

Two more magnetic structures and their corresponding spin-dependent polarized neutron reflectivity curves (after Ankner, Schreyer, Majkrzak, and Zabel).

New directions in science – synthetic superlattices

The same developments in physical vapor deposition methods were also being applied to the fabrication of composite layered systems (in some cases with atomic layer accuracy by molecular beam epitaxy) that do not occur in nature but which could be tailored to study fundamental physical phenomena in a controlled, systematic way.

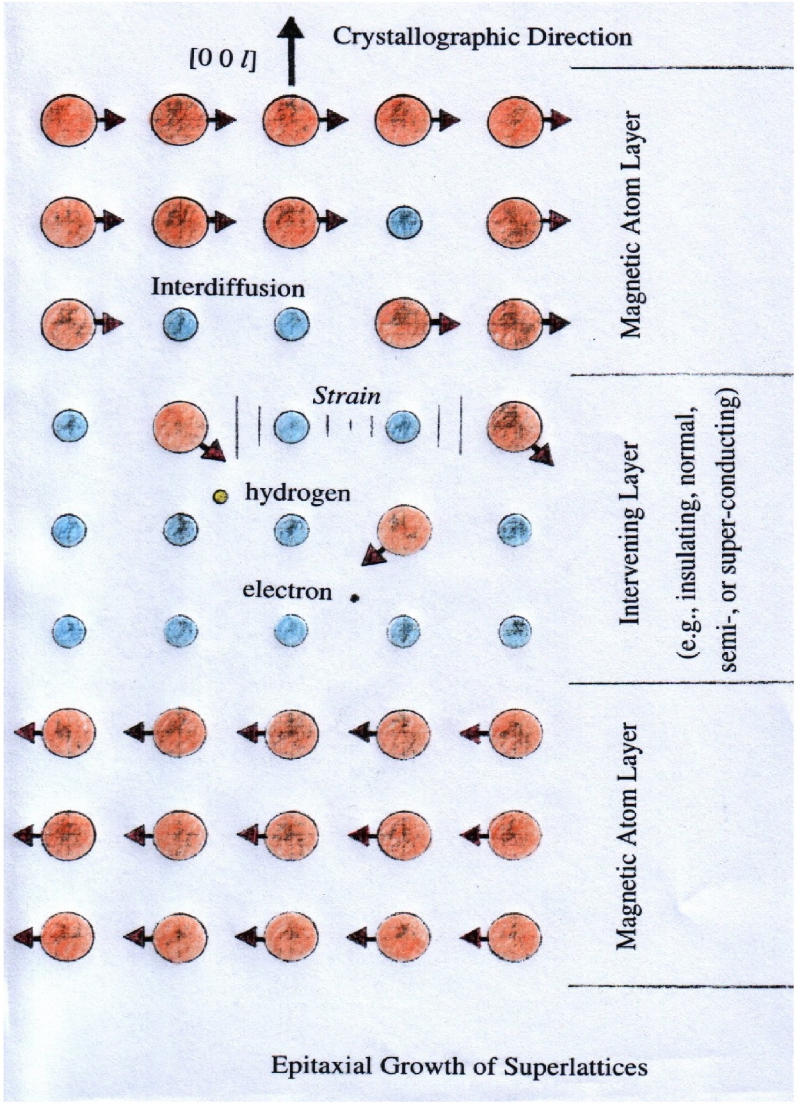

By means of molecular beam epitaxial growth in ultrahigh vacuum and other thin film deposition techniques, it is possible to construct synthetically layered systems tailored to study specific types of interactions of interest in hard condensed matter. For instance, how two separated regions made up of ferromagnetic atomic planes interact with one another across an intervening region of atomic planes of a material that is superconducting or semiconducting can be studied by analysis of the polarized neutron reflectivity -- as a function of temperature, applied magnetic field magnitude and direction, or other parameter such as the thickness of the intervening layer.

There exists a considerable body of work on systems prepared in this manner.

Superlattice structures of alternating layers of various rare earth elements such as Gd, Dy, Y, and Ho were found to have numerous interesting and sometimes relatively complicated magnetic structures and phase diagrams.

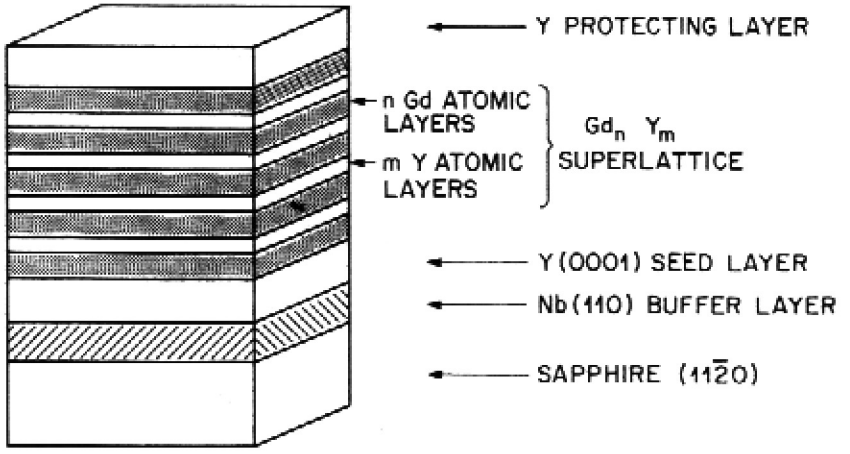

Figure 3. Schematic of typical growth process for a Gd_n–Y_m superlattice.

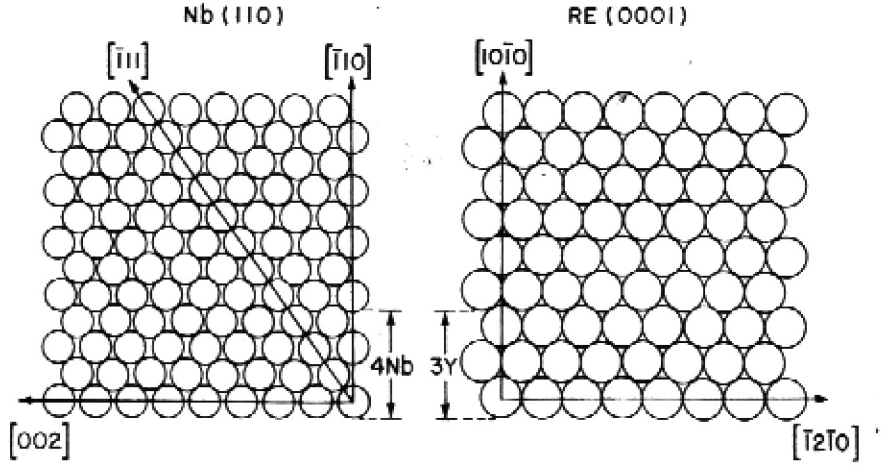

Figure 4. In-plane epitaxial structure between rare earth(0001) and Nb(110) crystals.

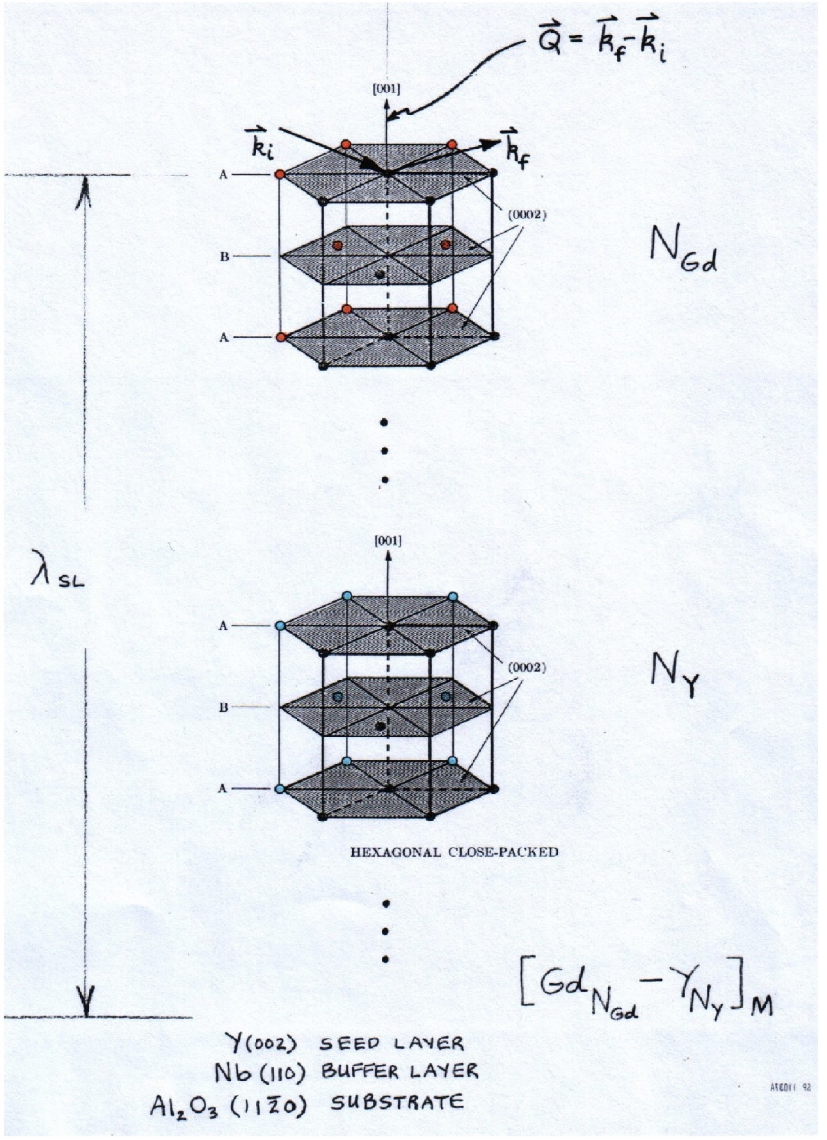

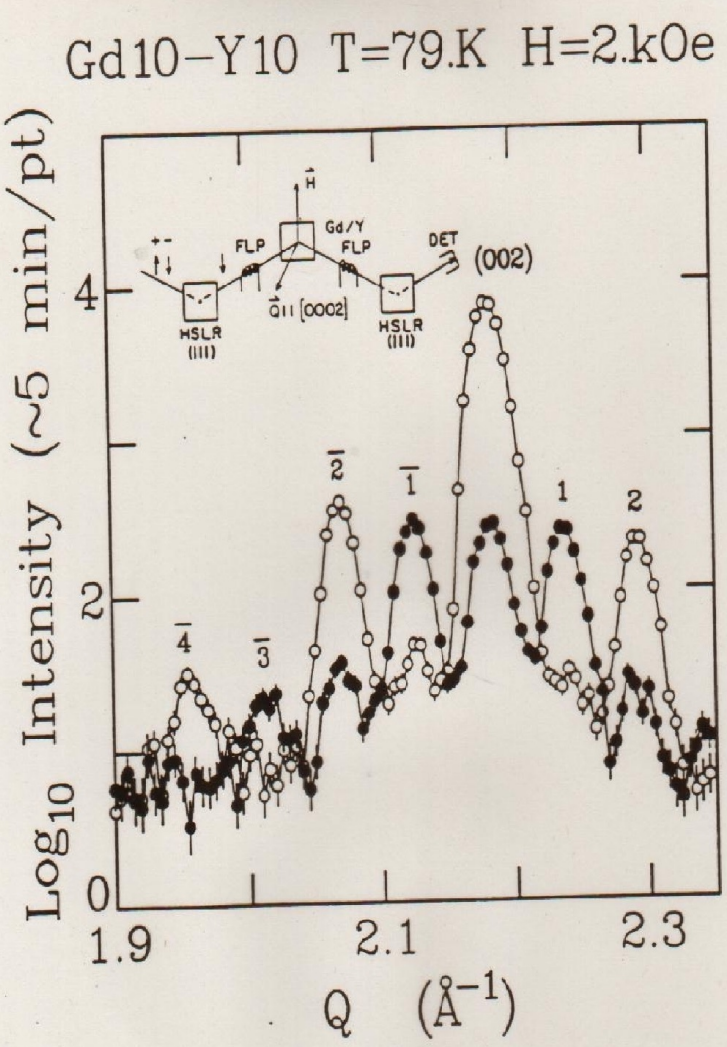

Fig. 7–1

Figure 7-1. NSF (open circles) and SF (filled circles) scattering from a [Gd_{10} - Y_{10}] superlattice as described in the text. The data have not been corrected for instrumental polarizing and flipping efficiencies (the SF scattering at the (002) position is predominantly, if not entirely, instrumental in origin). The SF scattering which appears at values of Q corresponding to a doubling of the chemical bilayer spacing (odd-numbered satellites) is consistent with an antiferromagnetic alignment (for an applied field approaching zero) of neighboring ferromagnetic Gd layers as depicted schematically in Figure 7-2. (After Majkrzak et al. (1986)).

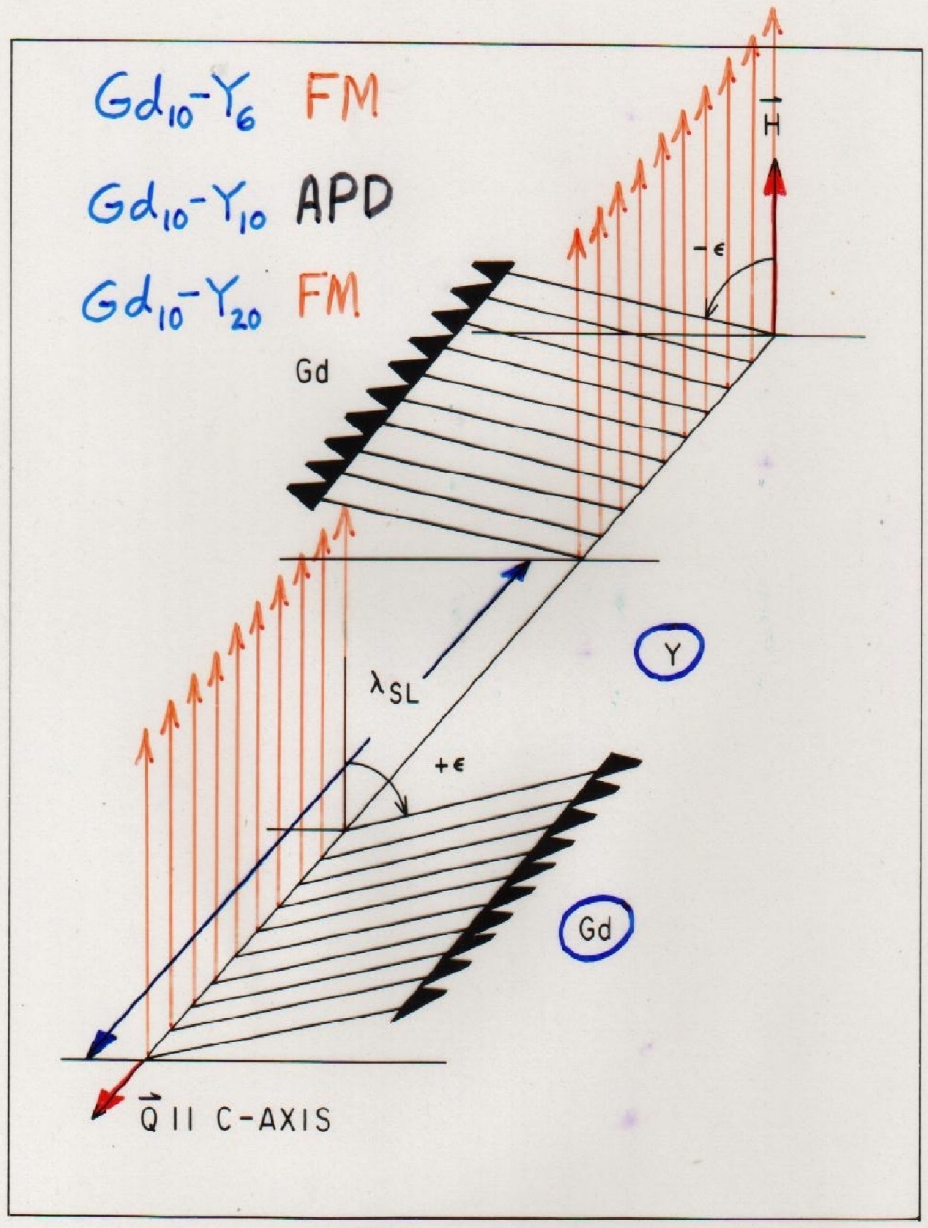

Part 3: The phase problem, direct inversion and simultaneous fitting -- including an example of how a unique solution for a physical structure can be obtained

<> ambiguous SLD profiles from reflected *intensities*

<> measurement of reflection *amplitude* via references yields unique solution -- one-to-one correspondence with SLD profile

<> given the reflection amplitude, exact, first-principles inversion to obtain unique SLD profile for specular reflection is possible

<> simultaneous fitting of multiple composite (sample + reference) reflectivity data sets can lead to unambiguous solution as well

The Phase Problem

In general, the probability of finding a neutron described by a wave function $\psi(z)$ at a position z is given by

$$\text{Probability}(z) = \psi(z)^{*}\psi(z) = |\psi(z)|^{2}$$

Therefore, for a wave function of the form $\psi(z) = A \exp(+ik_z z) = A[\cos(k_z z) + i \sin(k_z z)]$

$$\text{Probability}(z) = A^{*}\exp(-ik_z z)\, A \exp(+ik_z z) = |A|^{2}$$

-- all the phase information contained in the argument of the exponential function is lost!

And the only measurable quantity is the *reflectivity* $|r_{BA}(Q_Z)|^2 = r_{BA}(Q_Z)^{*} r_{BA}(Q_Z)$:

$$|r_{BA}(Q_Z)|^{2} \approx \left|[4\pi / (iQ_Z)] \int_{-\infty}^{+\infty} \rho(z) \exp(-iQ_z z)\, dz\right|^{2}$$

Two very different model scattering length density (SLD or ρ) depth profiles but which have one common layer segment (labeled “reference”).

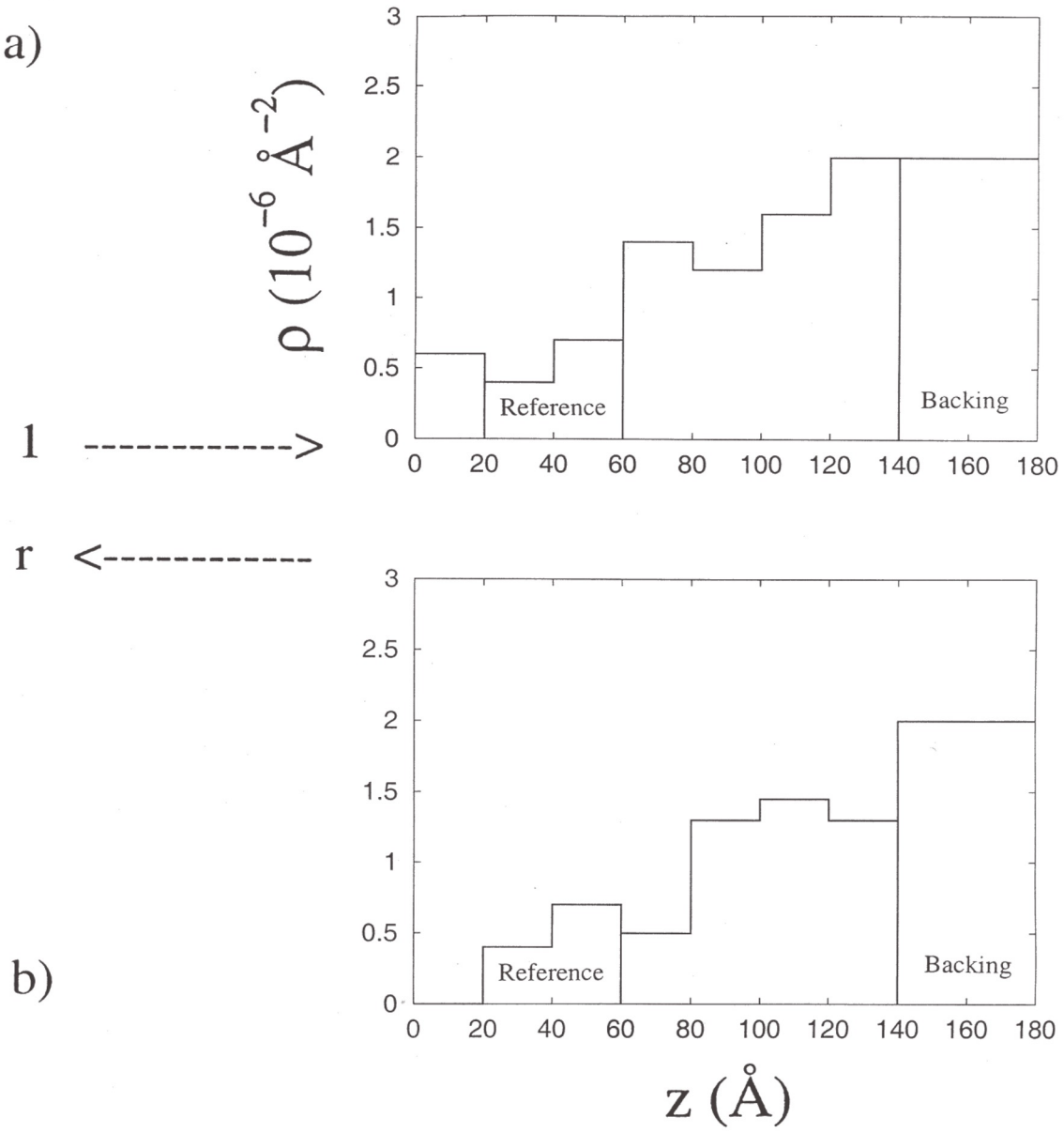

Figure 9.

Figure 10.

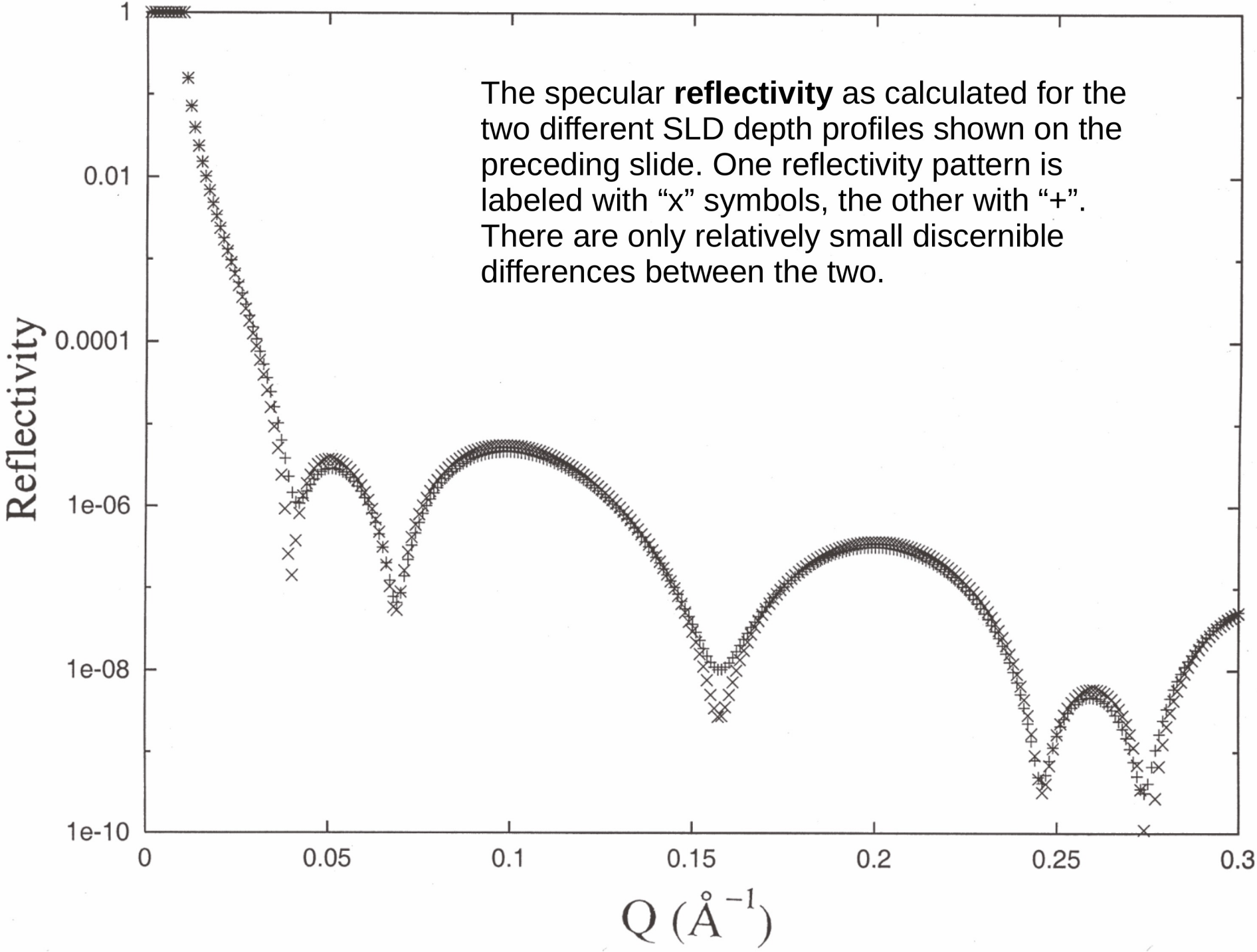

The specular **reflectivity** as calculated for the two different SLD depth profiles shown on the preceding slide. One reflectivity pattern is labeled with “x” symbols, the other with “+”. There are only relatively small discernible differences between the two.

Figure 11.

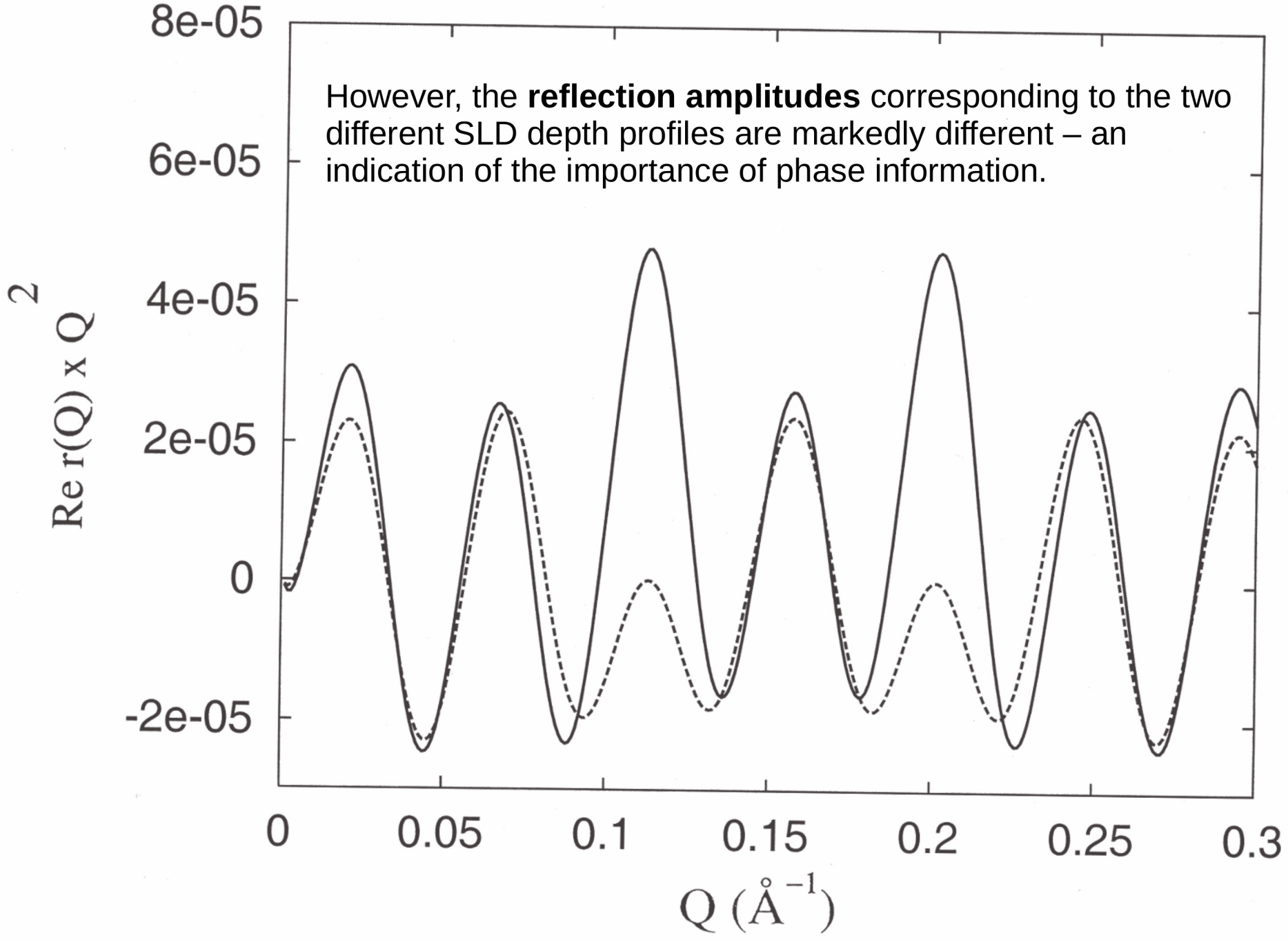

However, the **reflection amplitudes** corresponding to the two different SLD depth profiles are markedly different – an indication of the importance of phase information.

PBS

TiO in situ: Wiesler, et al.

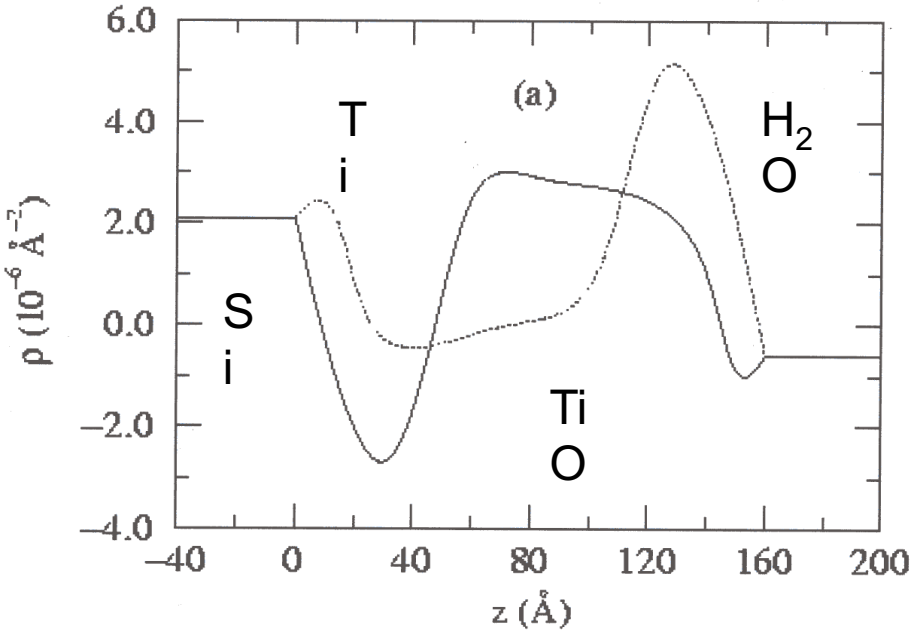

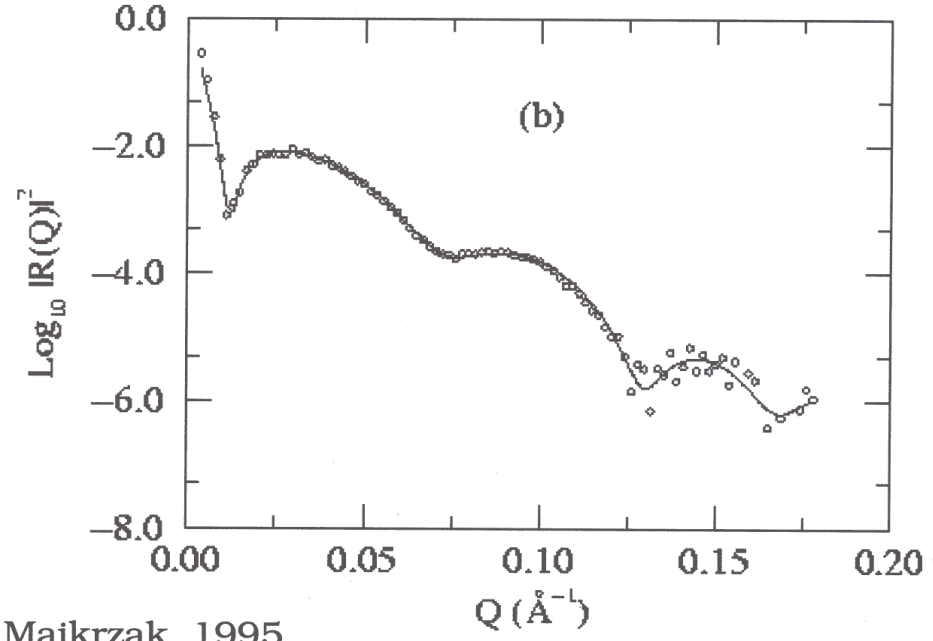

Berk & Majkrzak, 1995

Inverting reflectivity

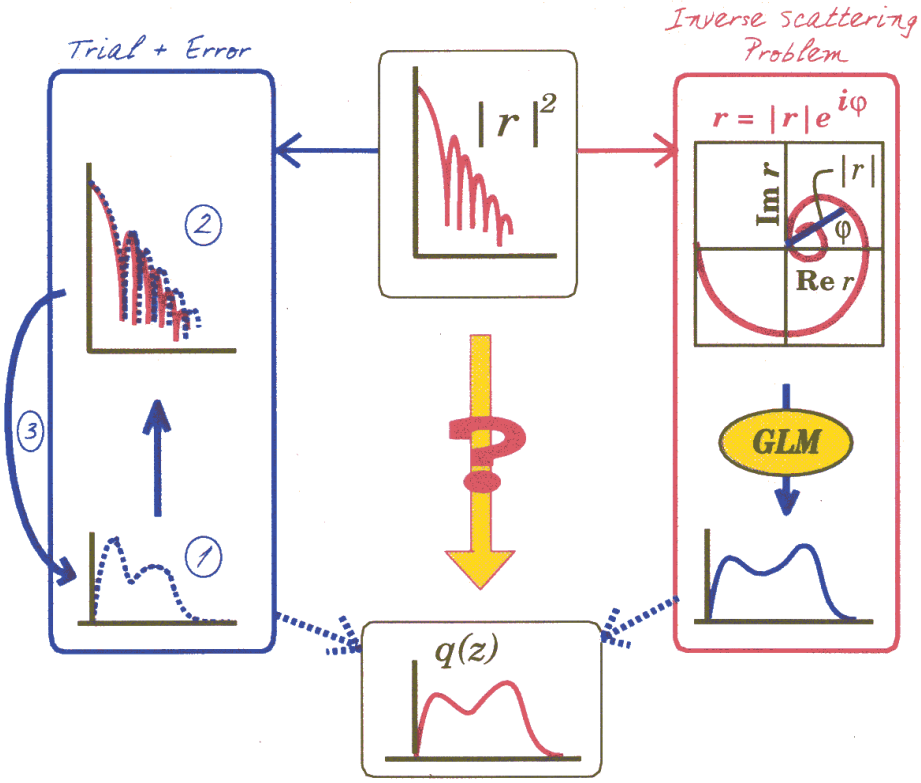

Phase determination
C.F. Majkrzak and N.F. Berk, Phys. Rev. B **52**, 10827 (1995).
V.–O. de Haan, et al., Phys. Rev. B **52**, 10830 (1995).

H. Leeb, H.R. Lipperheide and G. Reiss, this conference.

Logarithmic dispersion
W.L. Clinton, Phys. Rev. B **48**, 1 (1993).
Tunneling times
H. Fiedeldey, H.R. Lipperheide, et al., Phys. Lett. A **170**, 347 (1992).

Pseudo–inversion
S.K. Sinha, et al., *Surface X–Ray and Neutron Scattering*, 85 (Springer, 1992).
C.F. Majkrzak, N.F. Berk, et al., SPIE Proc. **1738**, 282 (1992).

NIST

Phase Determination with Surround Variation

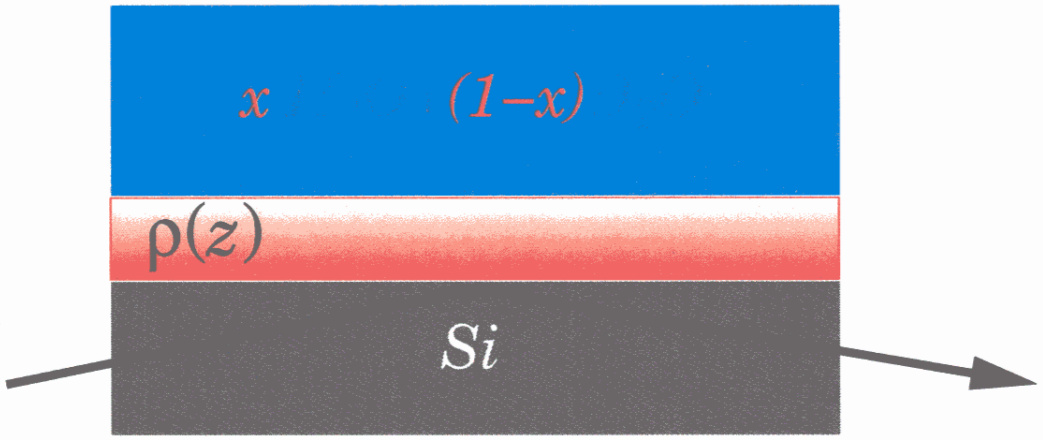

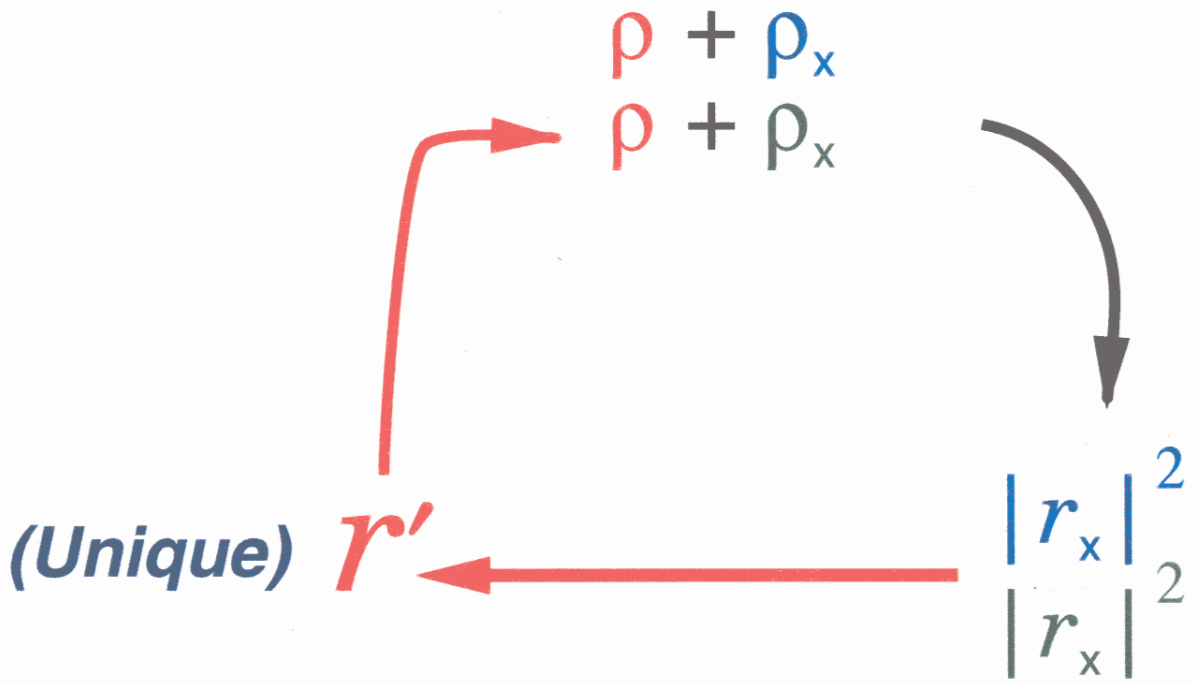

Majkrzak & Berk, 1998

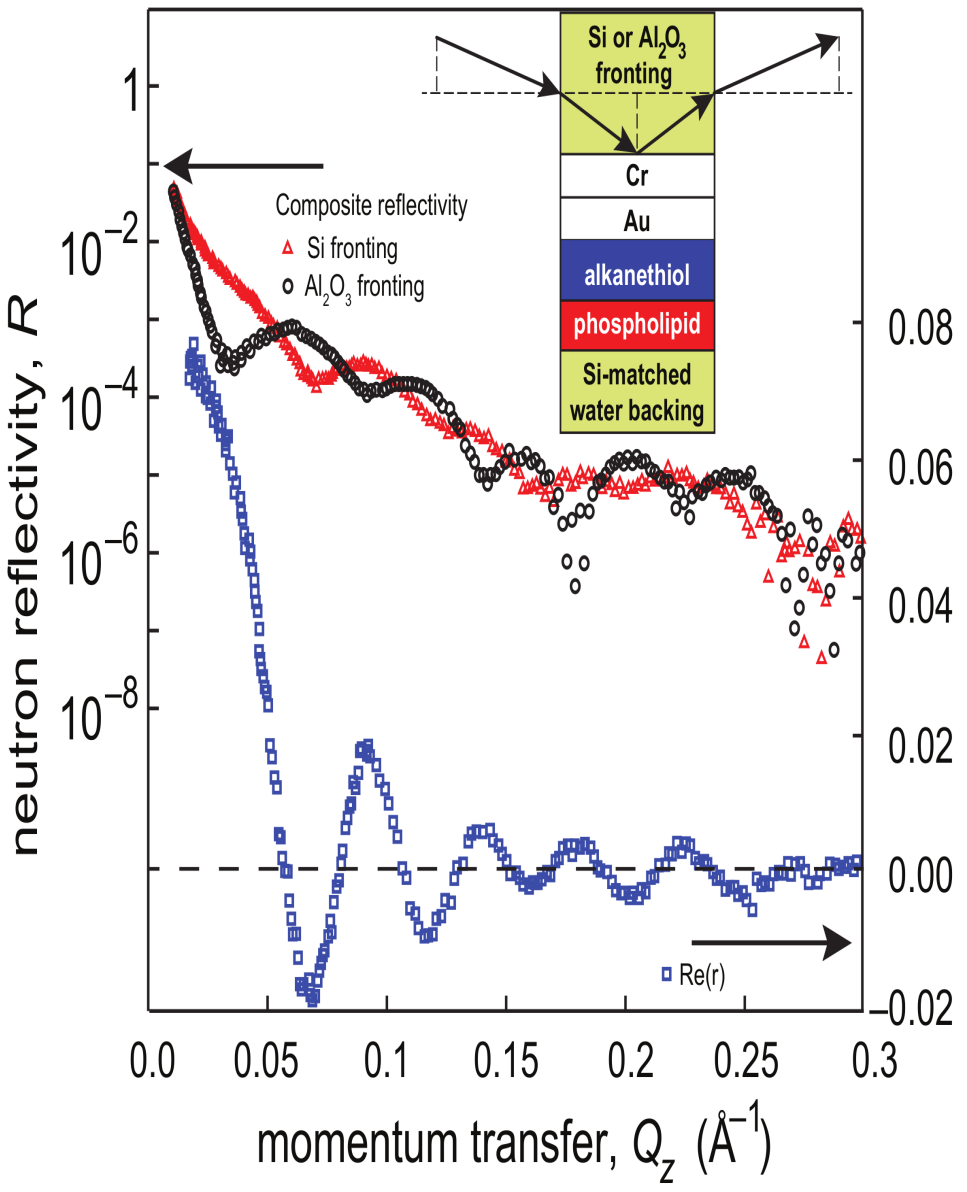
Si or Al2O3 fronting
Cr
Au
alkanethiol
phospholipid
Si-matched water backing
Composite reflectivity
Si fronting
Al2O3 fronting
Re(r)
neutron reflectivity, R
momentum transfer, Qz (Å−1)
1
10−2
10−4
10−6
10−8
0.08
0.06
0.04
0.02
0.00
−0.02
0.0
0.05
0.1
0.15
0.2
0.25
0.3

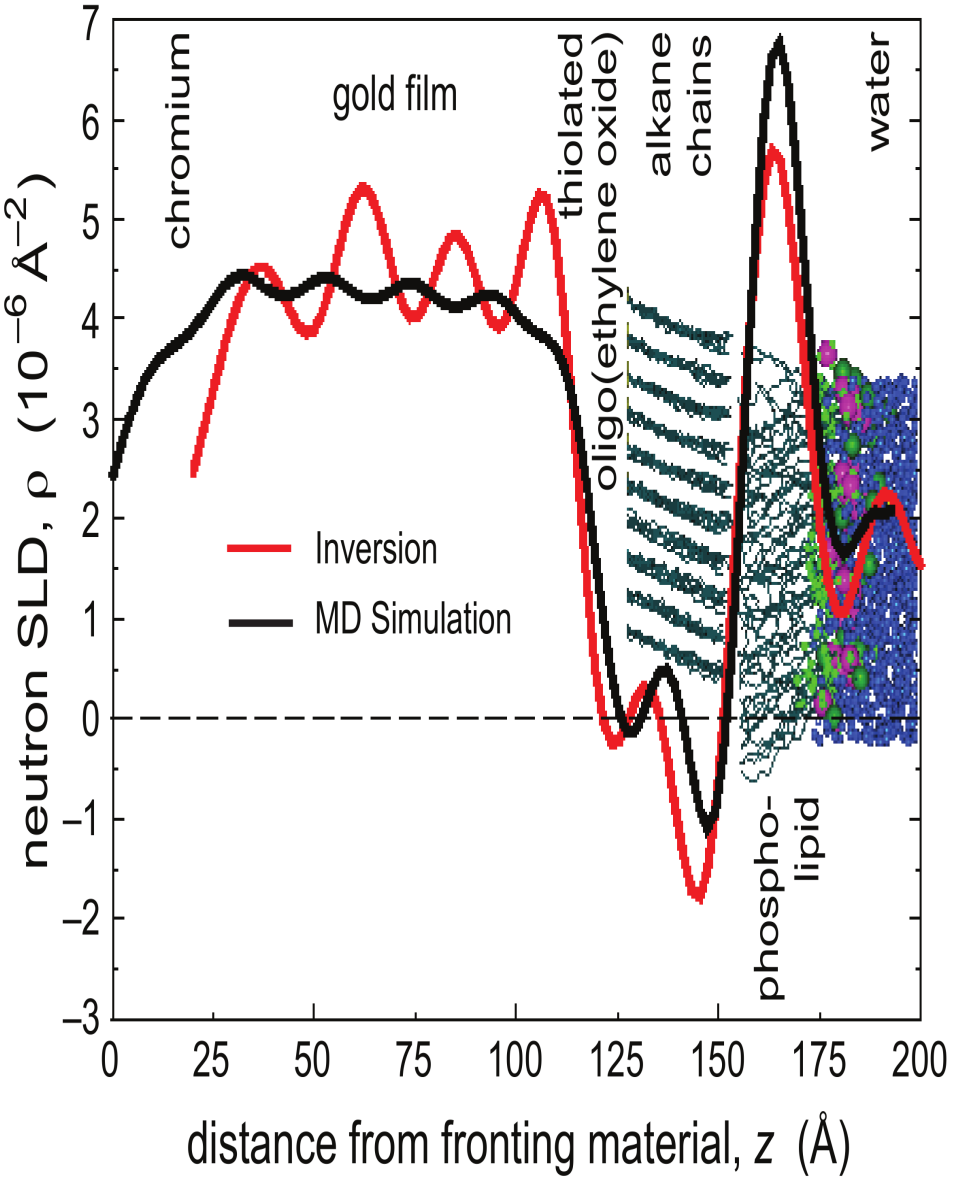
chromium
gold film
thiolated oligo(ethylene oxide)
alkane chains
water
phospho-lipid
Inversion
MD Simulation
neutron SLD, ρ (10−6 Å−2)
distance from fronting material, z (Å)
7
6
5
4
3
2
1
0
−1
−2
−3
0
25
50
75
100
125
150
175
200

Bibliography / References

Optics, 3rd Ed., by E. Hecht, Addison-Wesley, 1998.

Neutron Optics, by V.F. Sears, Oxford University Press, 1989.

Principles of Optics, 6th Ed., by M. Born and E. Wolf, Pergamon Press, 1987.

Quantum Mechanics, 2nd Ed., by E. Merzbacher, Wiley, 1970.

"Structural Investigations of Membranes in Biology by Neutron Reflectometry", C.F.Majkrzak, N.F.Berk, S.Krueger, and U.A.Perez-Salas, Chapter 12 in *Neutron Scattering in Biology*, Edited by J.Fitter, T.Gutberlet, and J.Katsaras, (Springer, Berlin, 2006) p.225-263.

"Polarized Neutron Reflectometry", C.F.Majkrzak, K.V.O'Donovan, and N.F.Berk, Chapter 9 in *Neutron Scattering from Magnetic Materials*, Edited by T.Chatterji, (Elsevier, Amsterdam, 2006) p.397-471.

"Phase-Sensitive Neutron Reflectometry", C.F.Majkrzak, N.F.Berk, and U.A.Perez-Salas, *Langmuir* **19**, 7796 – 7810 (2003).

B.J.Kirby et al., Phase-sensitive specular neutron reflectometry . . ., *Current Opinion in Colloid & Interface Science* **17** (2012) 44-53.

C.F.Majkrzak et al., *J. Appl. Phys.* **110** (2011).

www.ncnr.nist.gov -- look here for information about neutron reflectometry in general as well as in specific studies highlighted in past and current annual reports for the facility.